Redox Biology 47 (2021) 102163

Contents lists available at ScienceDirect

Redox Biology

journal homepage: www.elsevier.com/locate/redox

Novel role of xanthine oxidase-dependent H_2O_2 production in 12/15-lipoxygenase-mediated de novo lipogenesis, triglyceride biosynthesis and weight gain

Suresh Govatati [a], Prahalathan Pichavaram [a], Arul M. Mani [a], Raj Kumar [a], Deepti Sharma [a], Ari Dienel [a], Sunita Meena [a], Michelle A. Puchowicz [b], Edwards A. Park [c], Gadiparthi N. Rao [a,*]

[a] Department of Physiology, University of Tennessee Health Science Center, Memphis, TN, 38163, USA
[b] Department of Pediatrics, University of Tennessee Health Science Center, Memphis, TN, 38163, USA
[c] Department of Pharmacology, University of Tennessee Health Science Center, Memphis, TN, 38163, USA

ARTICLE INFO

Keywords:
12/15-Lipoxygenase
Xanthine oxidase
Hydrogen peroxide
de novo lipogenesis
Triglyceride biosynthesis
Weight gain

ABSTRACT

12/15-lipoxygenase (12/15-LOX) plays an essential role in oxidative conversion of polyunsaturated fatty acids into various bioactive lipid molecules. Although 12/15-LOX's role in the pathophysiology of various human diseases has been well studied, its role in weight gain is controversial and poorly clarified. Here, we demonstrated the role of 12/15-LOX in high-fat diet (HFD)-induced weight gain in a mouse model. We found that 12/15-LOX mediates HFD-induced de novo lipogenesis (DNL), triglyceride (TG) biosynthesis and the transport of TGs from the liver to adipose tissue leading to white adipose tissue (WAT) expansion and weight gain via xanthine oxidase (XO)-dependent production of H_2O_2. 12/15-LOX deficiency leads to cullin2-mediated ubiquitination and degradation of XO, thereby suppressing H_2O_2 production, DNL and TG biosynthesis resulting in reduced WAT expansion and weight gain. These findings infer that manipulation of 12/15-LOX metabolism may manifest a potential therapeutic target for weight gain and obesity.

1. Introduction

Obesity is one of the main global public health issues affecting ~30% of the world population [1]. Epidemiological data shows that obesity has a tight association with a wide variety of human pathologies like type 2 diabetes, metabolic syndrome, chronic kidney disease, hypertension, cardiovascular disease and cancer [2,3]. In addition, obesity leads to the development of various social and economic problems [4,5]. Diet-induced weight gain is one of the most common forms of obesity [6]. Although various anti-obesity drugs are currently available, most of them have several side effects, thus limiting their wider and long-term usage [7]. Therefore, there is a need for rigorous investigation to identify novel therapeutic targets for the development of efficient anti-obese drugs.

Lipoxygenases (LOXs) are nonheme iron-containing dioxygenases that are involved in oxidative metabolism of polyunsaturated fatty acids [8,9]. The human leukocyte type 12-LOX and reticulocyte type 15-LOX1, which are referred to as 12/15-LOX, generate similar products from common substrates [10,11]. Mice express only the leukocyte type 12-LOX, which is referred to as murine ortholog of human 12/15-LOX [12]. The murine 12-LOX converts arachidonic acid (AA) mainly to 12 (S)-HETE, whereas the human 15-LOX1 and 15-LOX2 convert AA mainly to 15(S)-HETE [11–13]. The role of 12/15LOX in various human pathologies has been well documented [9]. Specifically, we and others have shown a role for 12/15-LOX in atherogenesis [14–16]. In elucidating the mechanisms by which 12/15-LOX influences diet-induced atherogenesis, we observed that while C57BL/6J (wild type; WT) mice gained a substantial body weight, 12/15-LOX$^{-/-}$ mice (on C57BL/6J background) remained lean on high fat diet (HFD). In addition, it was reported that 12/15-LOX plays a role in steatohepatitis and weight gain using 12/15-LOX$^{-/-}$ mice on ApoE$^{-/-}$ background [17]. In another study, it was reported that 12/15-LOX deficiency (C57BL/6J background) without having any effect on weight gain plays a role in steatohepatitis [18]. In contrast, other studies using adipose tissue (AT)-specific 12/15-LOX$^{-/-}$ mice have reported a lack of a role for 12/15-LOX in weight gain [19]. Regardless of these conflicting observations, mice with 12/15-LOX deficiency have been shown to exhibit reduced AT inflammation and increased insulin sensitivity as compared to WT mice on HFD [20,21]. However, use of tissue-specific

* Corresponding author. Department of Physiology, University of Tennessee Health Science Center, 71 S Manassas street, Memphis, TN, 38163, USA.
E-mail address: rgadipar@uthsc.edu (G.N. Rao).

https://doi.org/10.1016/j.redox.2021.102163
Received 16 September 2021; Received in revised form 7 October 2021; Accepted 7 October 2021
Available online 12 October 2021

Abbreviations

ADP	adenosine diphosphate
AMP	adenosine monophosphate
AMPK	adenosine monophosphate-activated protein kinase
ATP	adenosine triphosphate
AP	allopurinol
AT	adipose tissue
BW	body weight
CD	chow diet
ACC1	acetyl coenzyme A carboxylase 1
CPT1B	carnitine palmitoyltransferase 1B
CREB	cyclic AMP-responsive element binding protein
DGAT2	diacylglycerol acyltransferase 2
DNL	de novo lipogenesis
DTT	dithiothreitol
Egr1	early growth response gene 1
FAS	fatty acid synthase
GTT	glucose tolerance test
12(S)-HETE	12-hydroxyeicosatetraenoic acid
HFD	high-fat diet
H_2O_2	hydrogen peroxide
INSIG1	insulin induced gene 1
ITT	insulin tolerance test
12/15-LOX	12/15-lipoxygenase
mTOR	mammalian target of rapamycin
OCT	optimal cutting temperature
PEPCK	phosphoenolpyruvate carboxykinase
RIPA bugger	Radioimmunoprecipitation assay buffer
SREBP1	sterol regulatory element-binding protein 1
TG	triglycerides
WAT	white adipose tissue
WT	wild type
XO	xanthine oxidase

12/15-LOX$^{-/-}$ mice for weight gain studies may not be appropriate as it may not affect 12(S)-HETE production by other tissues and thereby 12(S)-HETE circulating levels, which can still exert its effects on target tissues vis binding to its receptor GPR31 [22]. Thus, the role of 12/15-LOX in weight gain is unclear and needs further investigation.

In the present study, first, we confirmed the role of 12/15-LOX in HFD-induced weight gain in a mouse model. Then, in exploring the potential mechanisms, we found that 12/15-LOX plays a role in de novo lipogenesis (DNL) as well as triglyceride (TG) biosynthesis and its transport from liver to adipose tissue. We also found that HFD-induced 12/15-LOX-mediated DNL and TG biosynthesis leading to WAT expansion and weight gain requires xanthine oxidase (XO)-dependent H_2O_2 production. Furthermore, 12/15-LOX deficiency leads to cullin2-mediated ubiquitination and degradation of XO, which in turn, negates H_2O_2 production and its downstream signaling events such as INSIG1-mediated SREBP1c activation, ACC1 and FAS expression and DNL, p38MAPK-CREB-Egr1-mediated DGAT2 expression and TG biosynthesis, and ApoB100 induction. Together, these findings infer that 12/15-LOX plays a crucial role in lipid metabolism, particularly hepatic DNL and TG biosynthesis leading to epididymal WAT expansion and weight gain.

2. Results

2.1. 12/15-LOX plays a role in HFD-induced weight gain

In accordance with a previous report [17], we observed a requirement for 12/15-LOX in HFD-induced weight gain (Fig. 1A and B). Specifically, while WT mice gained substantial body weight, 12/15-LOX$^{-/-}$ mice remained lean on HFD (Fig. 1A and B). Similarly, 12/15-LOX deletion prevented HFD-induced increase in fat mass (Fig. 1C) as well as epididymal adipocyte size (Fig. 1D). However, lean mass was increased in 12/15-LOX$^{-/-}$ mice as compared to WT mice on HFD (Fig. 1C). Although there was no apparent change in food intake between WT and 12/15-LOX$^{-/-}$ mice fed CD or HFD (Fig. 1E), O_2 consumption, CO_2 production and heat generation (energy expenditure) were significantly higher in 12/15-LOX$^{-/-}$ mice as compared to WT mice fed HFD (Fig. 1F–H). Interestingly, respiratory exchange ratio (RER) in 12/15-LOX$^{-/-}$ mice was similar to WT on HFD, but lower as compared to WT on CD (Fig. 1I). These results infer that both WT and 12/15-LOX$^{-/-}$ mice on HFD are predominantly using fat as a primary energy source. Furthermore, we observed significantly elevated fasting blood glucose levels in WT mice as compared to 12/15-LOX$^{-/-}$ mice on HFD (Fig. 1J). In line with this observation, 12/15-LOX$^{-/-}$ mice showed increased glucose tolerance and insulin sensitivity as compared to WT mice fed HFD (Fig. 1K and L). In addition, 12/15-LOX deletion blunted HFD-induced plasma TG, total cholesterol, HDL and LDL levels (Fig. 1M–P). To determine the role of 12/15-LOX in mediating these metabolic events, we studied the effect of HFD on 12/15-LOX expression. As compared to CD, HFD induced 12/15-LOX expression both at mRNA and protein levels in epididymal white adipose tissue (WAT) of WT mice, and as expected its expression was not observed in 12/15-LOX$^{-/-}$ mice (Fig. 1Q).

2.2. 12/15-LOX deficiency prevents HFD-induced DGAT2 expression

To explore the potential mechanisms by which 12/15-LOX$^{-/-}$ mice remain lean on HFD, we sought to investigate the effect of HFD on enzymes involved in carbohydrate and lipid metabolism. While no differences were found in phosphoenolpyruvate carboxykinase (PEPCK) levels, acetyl coenzyme A carboxylase 1 (ACC1) levels were increased 4-fold in WAT of WT mice, but not in 12/15-LOX$^{-/-}$ mice on HFD (Fig. 2A). PEPCK is a key rate-limiting gluconeogenic enzyme [23], whereas ACC1 catalyzes the first rate-limiting step in de novo fatty acid synthesis [24]. In addition, the expression levels of carnitine palmitoyltransferase 1B (CPT1B), a rate-limiting enzyme of mitochondrial β-oxidation [25], appear to be decreased in WAT of WT but not in 12/15-LOX$^{-/-}$ mice in response to HFD feeding (Fig. 2A). Besides these observations, HFD induced mechanistic target of rapamycin (mTOR) phosphorylation and AMP-activated protein kinase (AMPK) dephosphorylation in WAT of only WT mice, but not 12/15-LOX$^{-/-}$ mice (Fig. 2B). AMPK/mTOR signaling plays an important role in adipogenesis and weight gain [26–29]. While AMPK is a sensor of cellular energy, mTOR plays a pivotal role in nutrient signaling [26,29]. Under nutrient rich conditions, mTOR gets activated and facilitates various anabolic pathways leading to weight gain [30,31]. On the other hand, AMPK is activated by increased ADP/AMP ratio and thereby influences cellular metabolism towards catabolic pathways to generate ATP [32]. Our findings agree with this view in WT mice, where feeding mice with HFD while activated mTOR, inactivated AMPK (Fig. 2B). Interestingly, 12/15-LOX deficiency suppressed HFD-induced mTOR activation and AMPK inactivation (Fig. 2B). Since mTOR is involved in lipogenesis [33] and both mTOR activation and fat mass expansion by HFD were suppressed in 12/15-LOX$^{-/-}$ mice, we suspected a role for 12/15-LOX in TG biosynthesis. It was well established that diacylglycerol acyltransferase 1 and 2 (DGAT1/2) play an important role in TG biosynthesis [34].

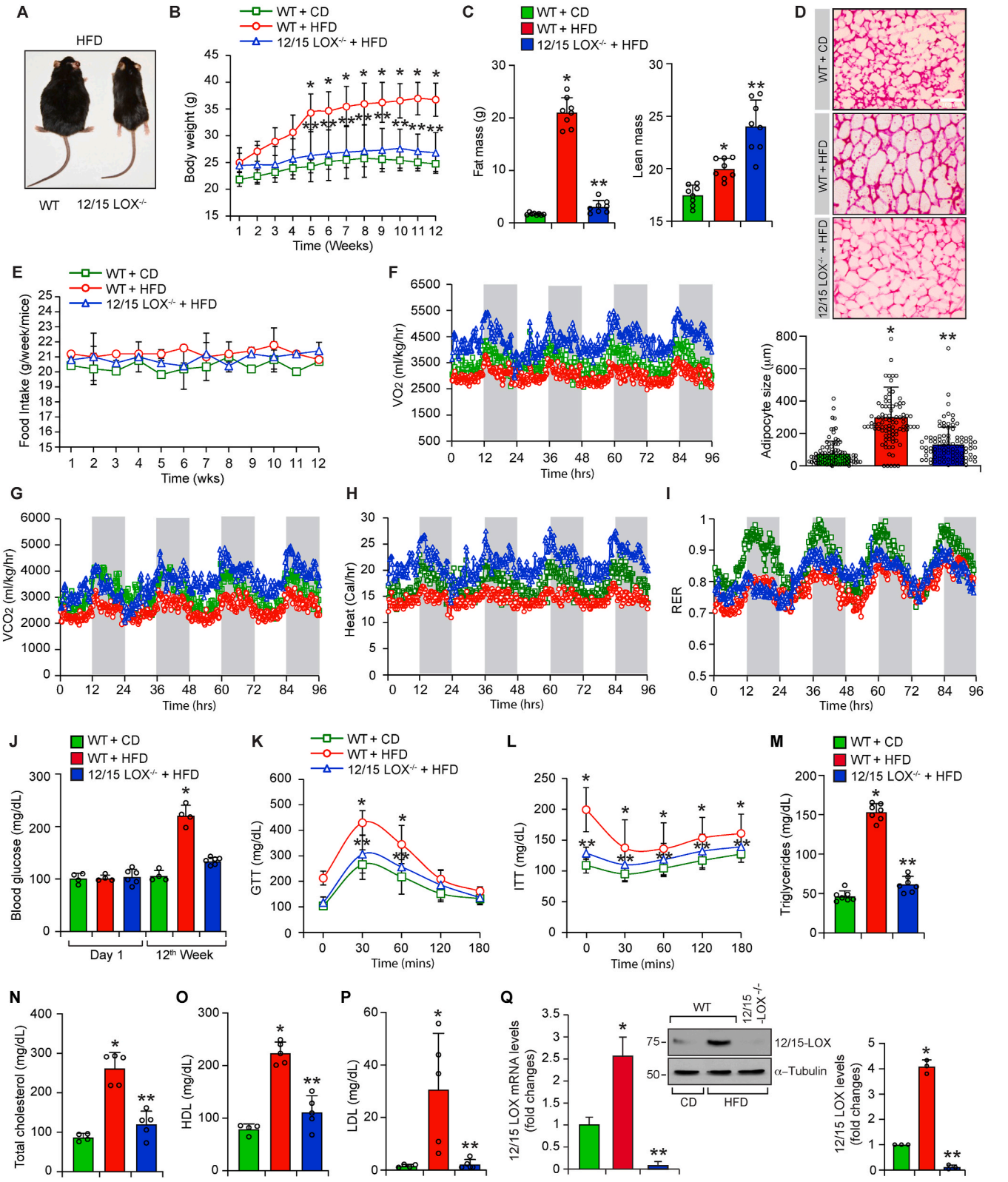

Fig. 1. 12/15-LOX deficiency prevents HFD-induced weight gain: A, Physical appearance of WT and 12/15-LOX$^{-/-}$ mice after 12 wks on HFD. B, Changes in body weight of mice at the indicated time periods (n = 7 in each group). C, Fat and lean mass weights of mice at 12th wk on the indicated diet via echoMRI. D, Changes in adipocyte size of mice after 12 wks on CD or HFD. E, Food intake per day at the indicated time intervals by WT and 12/15-LOX$^{-/-}$ mice fed with the indicated diet (n = 6 in each group). F–I, O_2 consumption (F), CO_2 production (G), heat generation (H) and respiratory exchange ratio (I) levels in WT and 12/15-LOX$^{-/-}$ mice fed CD or HFD for 12 wks (n = 8 in each group). J-L, Blood glucose levels at day 1 and after 12 wks on CD or HFD (J), glucose tolerance (K, n = 7 in each group) and insulin tolerance (L, n = 7 in each group). M – P, Plasma TG (M), total cholesterol (N), HDL (O), and LDL (P) levels of WT and 12/15-LOX$^{-/-}$ mice on CD or HFD for 12 wks. Q, 12/15-LOX expression at mRNA (left panel) and protein (right panel) levels in white adipose tissue (WAT) of WT and 12/15-LOX$^{-/-}$ mice fed CD or HFD for 12 wks *, $p < 0.05$ versus WT mice on CD; **, $p < 0.05$ versus WT mice on HFD.

Therefore, we measured the expression levels of DGAT1 and DGAT2. Our results showed that HFD while having no effect on DGAT1 expression induced DGAT2 expression only in WT but not 12/15-LOX$^{-/-}$ mice (Fig. 2C). To find whether DGAT2 induction occurs at transcriptional or posttranscriptional level, we tested the effect of HFD on DGAT2 mRNA levels. HFD induced DGAT2 mRNA levels 5-fold in WAT of WT mice but not 12/15-LOX$^{-/-}$ mice (Fig. 2D). These observations infer that 12/15-LOX plays a role in TG biosynthesis via inducing DGAT2 expression.

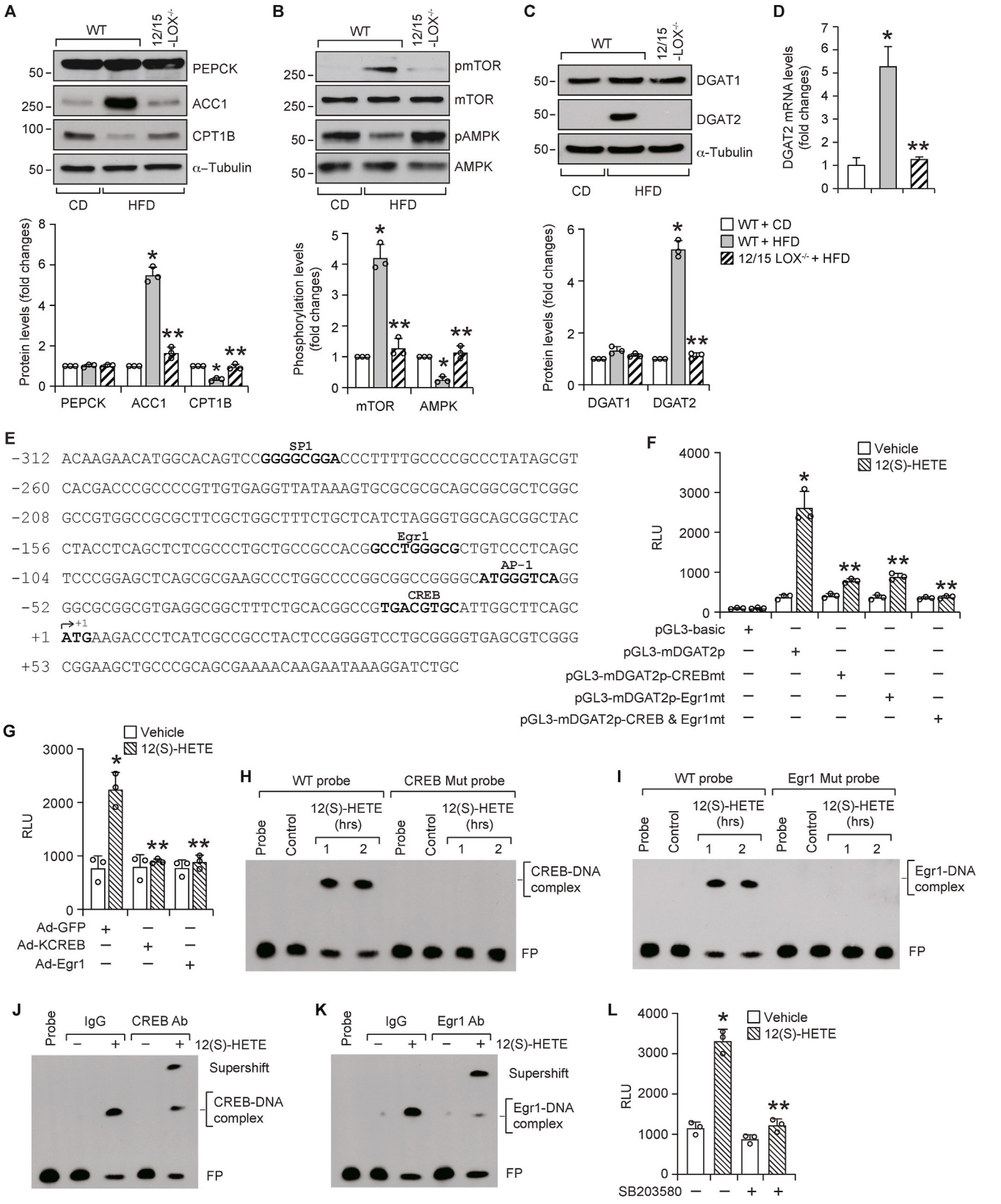

(caption on next page)

Fig. 2. 12/15-LOX deficiency prevents HFD-induced DGAT2 expression and 12/15-LOX dependent HFD-induced DGAT2 expression requires CREB and Egr1: A-C, Epididymal WAT extracts of CD-fed WT and 12 wks of HFD-fed WT and 12/15-LOX$^{-/-}$ mice were analyzed by western blotting for the indicated proteins using their specific antibodies. D, Relative mRNA expression levels of DGAT2 in WAT of CD-fed WT and 12 wks of HFD-fed WT and 12/15-LOX$^{-/-}$ mice. E, TRANSFAC analysis of mouse DGAT2 proximal promoter sequence encompassing from −312 nt to +92 nt for the identification of potential transcriptional factor binding sites. F, The effect of site-directed mutagenesis of CREB binding site at −12 nt and Egr1 binding site at −117 nt in pGL3-mDGAT2p construct on 12(S)-HETE (0.5 μM)-induced luciferase activity in 3T3-L1 adipocytes. G, 3T3-L1 adipocytes that were infected with Ad-GFP or Ad-KCREB or Ad-Egr1 were transfected with pGL3-mDGAT2p construct, treated with and without 12(S)-HETE (0.5 μM) for 1 h, and luciferase activity was measured. H and I, Time course effect of 12(S)-HETE (0.5 μM) on protein and mDGAT2 promoter DNA binding activity by EMSA using CREB binding element at −12 nt (H), and Egr1 binding element at −117 nt (I) as biotin labeled probes. J and K, Supershift EMSA analysis of nuclear extracts of control and 12(S)-HETE (0.5 μM)-treated 3T3-L1 adipocytes for CREB and Egr1 using CREB-binding element at −12 nt (J), and Egr1-binding element at −117 nt (K) as biotin labeled probes. L, 3T3-L1 adipocytes were transfected with pGL3-mDGAT2p construct, treated with and without 12(S)-HETE (0.5 μM) for 1 h in the presence or absence of SB203580 (10 μM) and luciferase activity was measured. *, $p < 0.05$ versus vehicle or WT mice on CD; **, $p < 0.05$ versus 12(S)-HETE or WT mice on HFD.

2.3. CREB and Egr1 mediate 12/15-LOX-dependent HFD-induced DGAT2 promoter activity

To explore the mechanisms by which 12/15-LOX triggers DGAT2 expression, we analyzed mouse DGAT2 (mDGAT2) proximal promoter sequence for potential transcription factor binding sites (TFBS) using TRANSFAC (TRANScription FACtor) software [35] (Fig. 2E). We found that mDGAT2 promoter contains one site for each of CREB (at −12 nt), AP-1 (at −55 nt), Egr1 (at −117) and SP1 (at −285 nt) (Fig. 2E). Based on this information, we cloned ~350 bp mDGAT2 proximal promoter into pGL3 basic vector (pGL3-mDGAT2p), transfected mouse 3T3-L1 adipocytes and its activity was measured in response to 12(S)-HETE, the major arachidonic acid metabolite of 12/15-LOX. 12(S)-HETE increased DGAT2 promoter activity 6-fold as compared to vehicle control (Fig. 2F). Recent studies have shown that both CREB and Egr1 play a role in obesity [36–39]. Therefore, we next tested the role of these transcriptional factors in 12(S)-HETE-induced mDGAT2 promoter activity by site-directed mutagenesis. Disruption of either CREB or Egr1 binding sites (Fig. S1) suppressed 12(S)-HETE-induced mDGAT2 promoter activity (Fig. 2F). To confirm these observations, we also studied the effects of the dominant negative mutants of CREB and Egr1 on 12(S)-HETE-induced mDGAT2 promoter activity. Blockade of either CREB or Egr1 by adenoviral-mediated expression of their dominant negative mutants completely inhibited 12(S)-HETE-induced mDGAT2 promoter activity (Fig. 2G). To obtain additional line of evidence for the role of CREB and Egr1 in 12(S)-HETE-induced mDGAT2 promoter activity, we next examined for the interaction of these transcriptional factors with mDGAT2 promoter by electrophoretic mobility shift assay (EMSA) using CREB-binding element at −12 nt and Egr1-binding element at −117 nt as biotin-labeled double-stranded oligonucleotide probes. We found that 12(S)-HETE induces CREB-DNA and Egr1-DNA binding activities in 3T3-L1 adipocytes (Fig. 2H and I). No protein-DNA binding activity was observed with either CREB or Egr1 mutant probes (Fig. 2H and I). To confirm the binding of CREB and Egr1 with mDGAT2 promoter, we also performed super-shift EMSA. As shown in Fig. 2J and K, the super-shift EMSA showed the presence of both CREB and Egr1 in the protein-DNA complexes induced by 12(S)-HETE.

2.4. p38MAPK mediates CREB-dependent Egr1 expression in the modulation of DGAT2 promoter activity

Since both CREB and Egr1 were involved in the modulation of mDGAT2 promoter activity by 12(S)-HETE, we wanted to explore the upstream mechanisms. A large body of data showed that p38MAPK plays a role in the phosphorylation and activation of CREB [40,41]. Based on these clues, we tested the role of p38MAPK in 12(S)-HETE-induced mDGAT2 promoter activity. SB203580, a specific inhibitor of p38MAPK [42] attenuated 12(S)-HETE-induced mDGAT2 promoter activity (Fig. 2L). To understand how p38MAPK mediates 12(S)-HETE-induced mDGAT2 promoter activity, we next studied its role in 12(S)-HETE-induced CREB activation and Egr1 expression. First, 12(S)-HETE stimulated phosphorylation of both p38MAPK and CREB in a time-dependent manner (Fig. 3A). Second, 12(S)-HETE induced the expression of Egr1 and DGAT2 in a time-dependent manner as well (Fig. 3B). Third, pharmacological inhibition of p38MAPK blocked 12(S)-HETE-induced CREB phosphorylation and Egr1 and DGAT2 expression (Fig. 3C and D). Since CREB and Egr1 directly bind and enhance mDGAT2 promoter activity and p38MAPK acts upstream to these signaling events, we questioned whether there is any crosstalk between CREB and Egr1. To this end, we found that siRNA-mediated depletion of CREB or blockade of its activation by its dominant negative mutant, Ad-KCREB, attenuated 12(S)-HETE-induced Egr1 and DGAT2 expression (Fig. 3E and F). In addition, blockade of Egr1 using its dominant negative mutant [43] inhibited 12(S)-HETE-induced DGAT2 expression (Fig. 3G). These results imply that p38MAPK-mediated CREB activation is required for Egr1 expression and that both CREB and Egr1 simultaneously are involved in enhancing mDGAT2 promoter activity leading to its expression by 12(S)-HETE. To validate these in vitro observations in vivo, we found that HFD induces p38MAPK and CREB phosphorylation as well as Egr1 expression in WAT of WT mice but not 12/15-LOX$^{-/-}$ mice (Fig. 3H–J).

2.5. XO-dependent H_2O_2 production is required for 12/15-LOX-induced p38MAPK-CREB-egr1-mediated DGAT2 expression

Many reports have shown that HFD generates reactive oxygen species (ROS) production [44,45]. Similarly, number of studies have reported that ROS, particularly H_2O_2 trigger p38MAPK activation [45–49]. Therefore, to explore the role of ROS in 12/15-LOX/12(S)-HETE-mediated p38MAPK-CREB-Egr1 signaling activation and DGAT2 expression, we first measured H_2O_2 production. HFD induced H_2O_2 production 4-fold in WAT of WT mice but not 12/15-LOX$^{-/-}$ mice (Fig. 4A). Since xanthine oxidase (XO) plays a predominant role in H_2O_2 production [50], we next tested the role of XO in HFD-induced H_2O_2 production. Feeding mice with HFD along with Allopurinol (AP), a specific inhibitor of XO [51], suppressed HFD-induced H_2O_2 production in WAT of WT mice (Fig. 4B). AP also blocked HFD-induced p38MAPK and CREB phosphorylation as well as Egr1 and DGAT2 expression (Fig. 4C–E). In line with these observations, AP inhibited 12(S)-HETE-induced p38MAPK and CREB phosphorylation and Egr1 and DGAT2 expression in 3T3-L1 adipocytes (Fig. 4F and G). To understand the mechanisms by which the lack of 12/15-LOX prevents H_2O_2 production, we measured XO expression levels. First, HFD induced XO expression at mRNA levels in WAT of both WT and 12/15-LOX$^{-/-}$ mice (Fig. 4H). However, XO expression at protein level occurred only in WT mice but not 12/15-LOX$^{-/-}$ mice (Fig. 4I). Based on these observations, we wanted to find whether XO is undergoing proteolytic degradation in 12/15-LOX$^{-/-}$ mice. We found that in 12/15-LOX$^{-/-}$ mice, XO was ubiquitinated in response to HFD feeding (Fig. 4J). Since cullin-RING family of ubiquitin ligases are expressed abundantly in adipose tissue and play an important role in adipogenesis [52], we next tested their role in XO ubiquitination. We found that cullin2 but not cullin1 or cullin3 binds to XO in WAT of 12/15-LOX$^{-/-}$ mice fed with HFD (Fig. 4K). These observations infer that XO-mediated H_2O_2 production via activation of p38MAPK-CREB-Egr1 signaling leads to DGAT2 expression downstream to 12/15-LOX/12(S)-HETE axis. In addition,

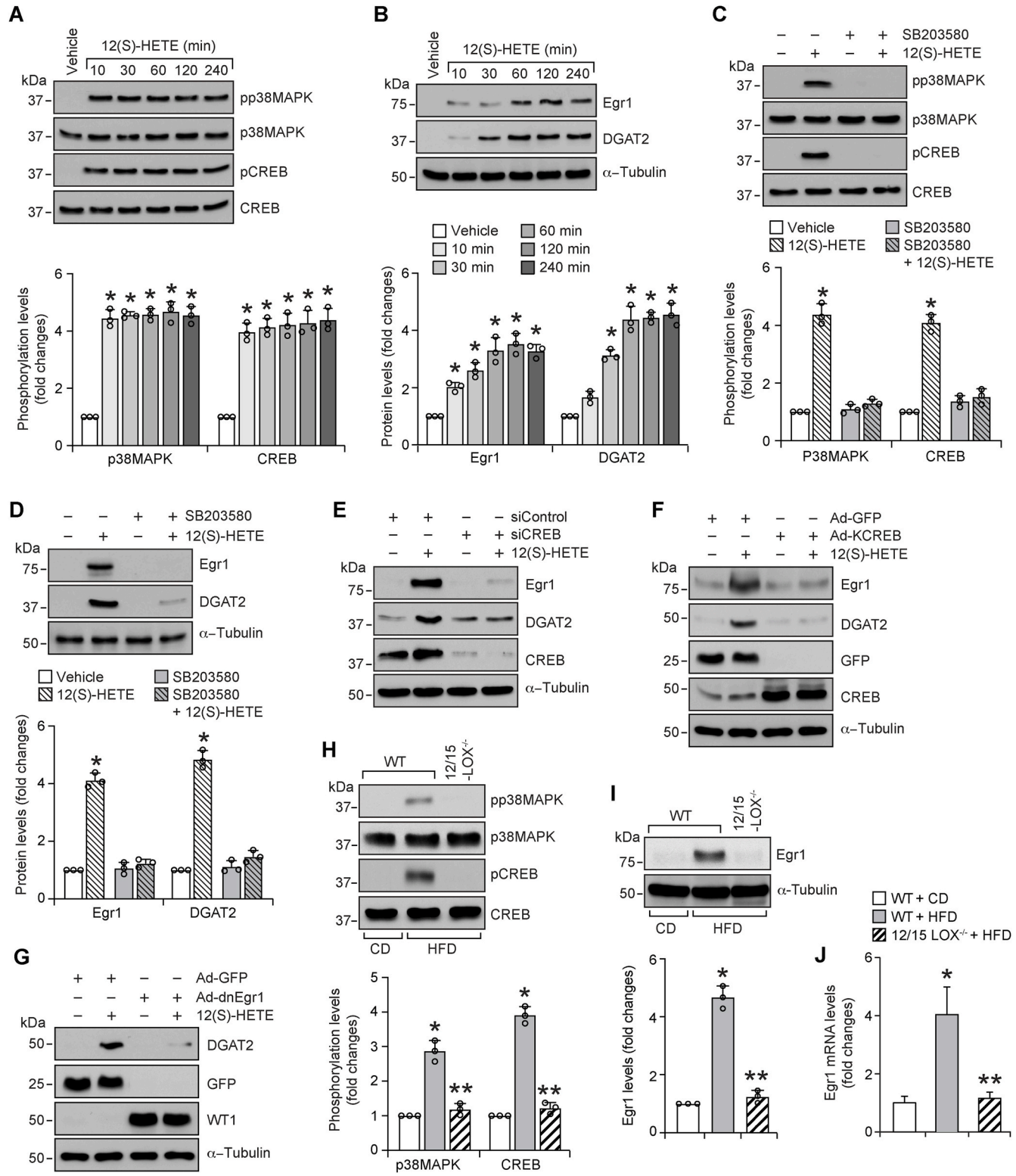

Fig. 3. p38MAPK-CREB-Egr1 signaling is required for 12(S)-HETE induced DGAT2 expression: A and B, 3T3-L1 adipocytes were growth-arrested, treated with and without 12(S)-HETE (0.5 μM) for indicated time periods and cell extracts were prepared and analyzed by western blotting for the indicated proteins using their specific antibodies. C and D, Growth-arrested 3T3-L1 adipocytes were treated with and without 12(S)-HETE (0.5 μM) in the presence or absence of SB203580 (10 μM) for 10 min (C) or 1 h (D) and cell extracts were prepared and analyzed by western blotting for the indicated proteins using their specific antibodies. E-G, 3T3-L1 adipocytes that were transfected with siControl or siCREB (100 nmoles) (E), or infected with Ad-GFP or Ad-KCREB or Ad-Egr1 (40 moi) (F and G), and growth-arrested were treated with and without 12(S)-HETE (0.5 μM) for 1 h and cell extracts were prepared and analyzed by western blotting. The efficacy of siCREB was shown by its effect on CREB levels and over-expression of the vectors for GFP, KCREB and dn-Egr1 was shown by probing for their expression levels. H and I, White adipose tissue extracts of CD-fed WT and 12 wks of HFD-fed WT and 12/15-LOX$^{-/-}$ mice were analyzed by western blotting for the indicated proteins using their specific antibodies. J, Relative mRNA expression levels of Egr1 in WAT of CD-fed WT and 12 wks of HFD-fed WT and 12/15-LOX$^{-/-}$ mice. *, $p < 0.05$ versus vehicle or WT mice on CD; **, $p < 0.05$ WT mice on HFD. WT1, Wilmer tumor protein 1.

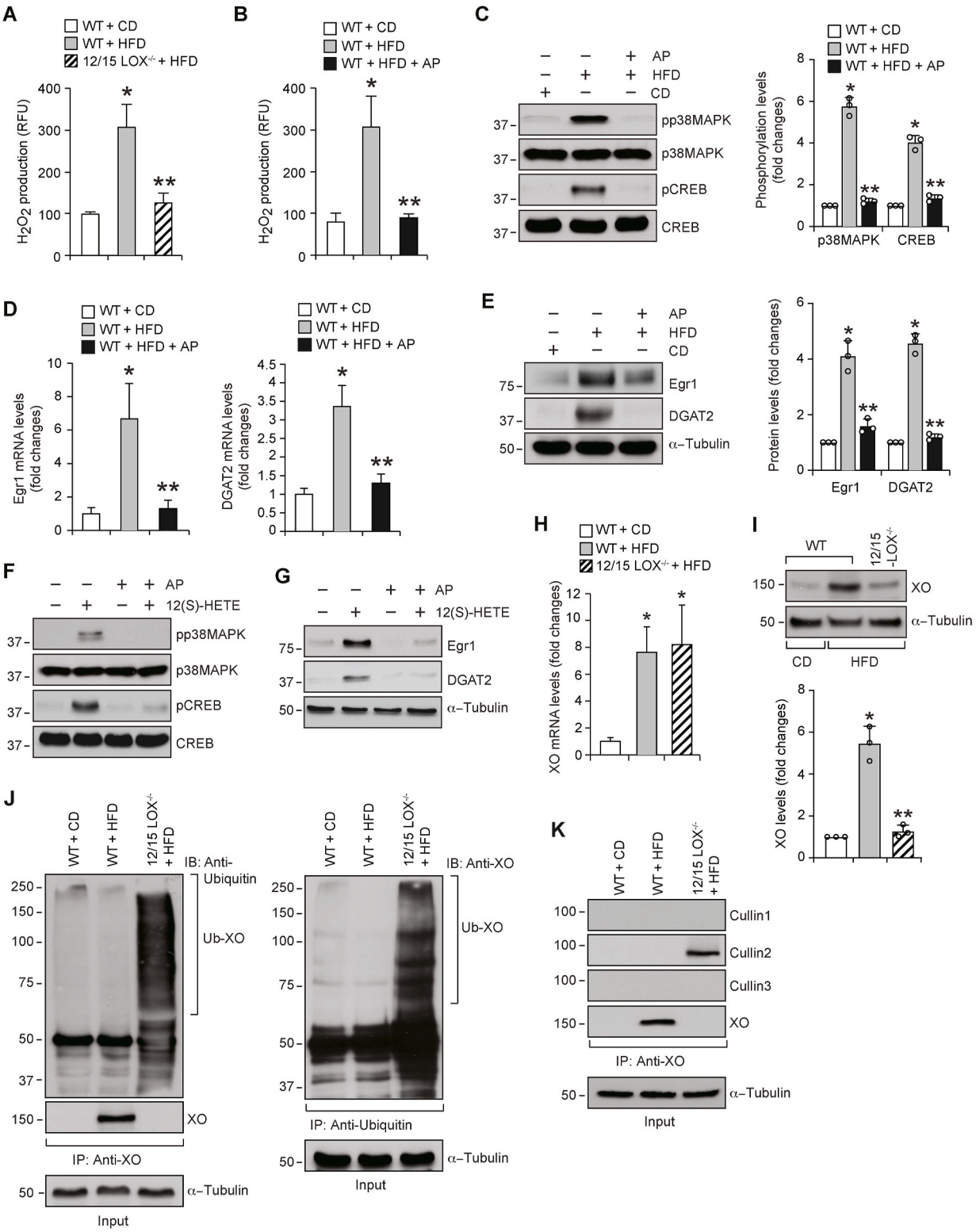

Fig. 4. XO-dependent H_2O_2 production is required for 12/15-LOX-induced p38MAPK-CREB-Egr1-mediated DGAT2 expression: A, H_2O_2 production in WAT of CD-fed WT and 12 wks of HFD-fed WT and 12/15-LOX$^{-/-}$ mice was measured using Amplex Red. B, WAT from WT mice fed with CD or HFD in combination with and without Allopurinol (125 mg/L of drinking water) for 12 wks were analyzed for H_2O_2 production using Amplex Red. C-E, WAT in panel B were analyzed by western blotting (C and E) and qRT-PCR (D) for protein levels and relative mRNA levels, respectively, of the indicated molecules. F and G, Growth-arrested 3T3-L1 adipocytes were treated with and without 12(S)-HETE (0.5 μM) in the presence or absence of Allopurinol (50 μM) for 10 min (F) or 1 h (G) and cell extracts were prepared and analyzed by western blotting for the indicated proteins using their specific antibodies. H and I, WT and 12/15-LOX$^{-/-}$ mice were fed with CD or HFD for 12 wks, and mRNA and protein levels of XO were measured by qRT-PCR (H) and Western blot analysis (I). J and K, WAT extracts containing equal amounts of protein from each regimen were immunoprecipitated with the indicated antibodies and the immunocomplexes were analyzed by western blotting for the indicated proteins using their specific antibodies. *, $p < 0.05$ versus WT mice on CD; **, $p < 0.05$ versus WT mice on HFD.

these observations reveal for the first time that XO undergoes cullin2-mediated ubiquitination and degradation in the absence of 12/15-LOX in response to HFD feeding. Corroborating these findings, AP attenuated HFD-induced weight gain, fat mass expansion, lean mass, blood glucose levels and improved glucose tolerance as well as insulin sensitivity with reduced plasma TG, total cholesterol and LDL levels in WT mice (Fig. 5A-M and O). However, AP had no effect on plasma HDL levels (Fig. 5N).

2.6. 12/15-LOX mediates HFD-induced SREBP1c activation, and ACC1 and FAS expression leading to increased DNL and TG biosynthesis in the liver

Although WAT expansion was increased substantially in HFD-fed WT mice as compared to 12/15-LOX$^{-/-}$ mice, no differences were observed in WAT TG levels of these mice on a unit basis (Fig. 6A). Since TG are synthesized in the liver and transported to adipose tissue for storage [53], we sought to investigate the role of 12/15-LOX in DNL and TG biosynthesis in the liver. First, we found that HFD induces hepatic TG levels manyfold in WT mice as compared to 12/15-LOX$^{-/-}$ mice (Fig. 6B). Second, we measured hepatic DNL and TG biosynthesis using $^{2}H_2O$-labeling followed by GC-MS analysis. Hepatic DNL and TG biosynthesis as measured by TG-bound ^{2}H-labeled fatty acid (FA) and TG-bound ^{2}H-labeled glycerol, respectively, were increased severalfold in WT mice as compared to 12/15-LOX$^{-/-}$ mice on HFD (Fig. 6C). In understanding the mechanisms involved in hepatic DNL, we also studied the effect of HFD on the expression of genes involved in DNL. HFD while having no effect on INSIG1/2 and SREBP1c mRNA levels induced ACC1 and FAS expression at both mRNA and protein levels by several fold in WT mice as compared to their levels in CD-fed WT mice (Fig. 6D and E). HFD caused downregulation of INSIG1 and induced SREBP1c cleavage in the livers of WT mice at protein level (Fig. 6E). However, HFD did not affect either mRNA or protein levels of these genes in 12/15-LOX$^{-/-}$ mice as compared to CD-fed WT mice (Fig. 6D and E). To explore the mechanisms underlying HFD-induced downregulation of INSIG1 levels, we examined its ubiquitination. HFD induced ubiquitination and degradation of INSIG1 only in WT mice but not 12/15-LOX$^{-/-}$ mice (Fig. 6F). Interestingly, HFD-induced increases in hepatic TG levels, DNL, and ACC1 and FAS expression as well as INSIG1 ubiquitination and SREBP1c cleavage were all negated by AP (Fig. 6B, C, G and I). In regard to mechanisms involved in hepatic TG biosynthesis, we found that HFD induces p38MAPK and CREB phosphorylation as well as Egr1 and DGAT2 expression in WT mice but not 12/15-LOX$^{-/-}$ mice (Fig. S2). In addition, we found that HFD induces XO expression in the livers of WT mice (Fig. 7A, B and E) and that it undergoes cullin2-mediated ubiquitination in 12/15-LOX$^{-/-}$ mice (Fig. 7C and D). Furthermore, inhibition of XO by AP blunted HFD-induced p38MAPK and CREB phosphorylation and Egr1 and DGAT2 expression (Fig. 7F–H).

2.7. H_2O_2 but not uric acid regulates HFD-induced 12/15-LOX-mediated hepatic DNL and TG synthesis

As our results showed that XO acts upstream to SREBP1c-mediated DNL and p38MAPK-CREB-Egr1-mediated TG biosynthesis and because XO produces both uric acid and H_2O_2 [50], we wanted to find which of these two molecules are involved in mediating these effects. To this end, we found that H_2O_2 but not uric acid induces ubiquitination and degradation of INSIG1, activation of SREBP1c and enhances the expression of ACC1 and FAS in mouse hepatocytes (Fig. 8A and B). Similarly, we observed that H_2O_2 stimulates p38MAPK and CREB phosphorylation and Egr1 and DGAT2 expression in mouse hepatocytes (Fig. 8C and D). Together, these findings infer that XO-mediated H_2O_2 production rather than uric acid plays an important role in HFD-induced DNL and TG biosynthesis in the liver. VLDL plays an important role in the transport of TG from liver to adipose tissue and ApoB100 is critical component of VLDL [54]. Therefore, to test whether 12/15-LOX influences TG transport from liver to adipose tissue, we studied the effect of HFD on ApoB100 expression. HFD while inducing the expression of ApoB100 at both mRNA and protein levels in the livers of WT mice, had no effect in 12/15-LOX$^{-/-}$ mice (Fig. 8E). Similarly, AP suppressed HFD-induced ApoB100 expression in the livers of WT mice (Fig. 8F).

In order to find why 12/15-LOX$^{-/-}$ mice remain lean on HFD, we measured their physical activity. While both WT and 12/15-LOX$^{-/-}$ mice on HFD were found to be equally active during the light cycle, WT mice on HFD were found to be less active than 12/15-LOX$^{-/-}$ mice during the dark cycle (Fig. 8G). Similarly, inhibition of XO by AP restored physical activity in WT mice on HFD (Fig. 8G).

3. Discussion

Previously it was reported that disruption of 12/15-LOX gene (on ApoE$^{-/-}$ background) prevents weight gain as compared to ApoE$^{-/-}$ mice on HFD [17]. However, other studies using either global or AT-specific 12/15-LOX$^{-/-}$ mice have reported no role for 12/15-LOX in weight gain in response to HFD feeding [18,19]. In any case, use of tissue-specific 12/15-LOX$^{-/-}$ mice for weight gain studies may not be appropriate as it may not affect 12(S)-HETE production by other tissues and thereby 12 (S)-HETE circulating levels, which can still exert its effects on target tissues vis binding to its receptor GPR31 [22]. Thus, the role of 12/15-LOX in weight gain is unclear. In the course of exploring the mechanisms of 12/15-LOX's role in atherosclerosis, we observed that while WT mice gained substantial body weight, 12/15-LOX$^{-/-}$ mice remained lean on HFD. Therefore, we conducted an in-depth mechanistic investigation to explore the 12/15-LOX's role in weight gain and its therapeutic potential in the prevention of weight gain and obesity. We found no apparent changes in food intake between WT and 12/15-LOX$^{-/-}$ mice fed with CD or HFD. However, O_2 consumption, CO_2 production and heat generation were significantly higher in 12/15-LOX$^{-/-}$ mice as compared to WT mice fed with HFD. These results indicate that the rate of energy expenditure in 12/15-LOX$^{-/-}$ mice is more than WT mice on HFD. Although, both WT and 12/15-LOX$^{-/-}$ mice are utilizing fat as a primary energy source on HFD, the increased rate of fat consumption in 12/15-LOX$^{-/-}$ mice may explain the resistance of these mice to weight gain. As WT mice are burning less fat as compared to 12/15-LOX$^{-/-}$ mice, the excess fat in these mice appears to be accumulated in WAT leading to its expansion, and this view can be corroborated by the finding that in WT mice the fat mass is substantially more than in 12/15-LOX$^{-/-}$ mice on HFD. This inference can be further supported by the observation that β-oxidation is low in HFD-fed WT mice as compared to CD-fed WT mice or HFD-fed 12/15-LOX$^{-/-}$ mice as measured by CPT1B expression. In line with these observations, WT mice developed dyslipidemia resulting in decreased insulin sensitivity and increased glucose tolerance. Furthermore, increased mTOR and decreased AMPK activation in WT mice as compared to 12/15-LOX$^{-/-}$ mice may also indicate that WT mice, although having excess nutrients, they are not being utilized for energy expenditure, suggesting that these mice might be less active on HFD. In fact, WT mice on HFD were found to be less active than 12/15-LOX$^{-/-}$ mice. These observations may also explain the high energy expenditure and heat production in 12/15-LOX$^{-/-}$ mice than WT mice on HFD. The increased ACC1 and DGAT2 expression in WT mice suggests that fatty acids are synthesized from carbohydrates and utilized for generation of TG leading to WAT expansion in these mice as compared to 12/15-LOX$^{-/-}$ mice.

Adipocytes are involved in lipid storage as well as the transport of lipids to other tissues and excessive accumulation of TG in WAT leads to obesity [55]. DGATs are enzymes that catalyze the formation of TG from diacylglycerol and activated forms of fatty acids (fatty acyl-CoAs) [56,57]. DGATs catalyze the terminal step in TG biosynthesis and thus are critical players in WAT expansion [58]. Between the two DGATs (DGAT1 and DGAT2) identified thus far [59,60], mice lacking DGAT1 are viable and resistant to HFD-induced obesity, exhibited increased energy expenditure and showed sensitivity to insulin and leptin [58,61],

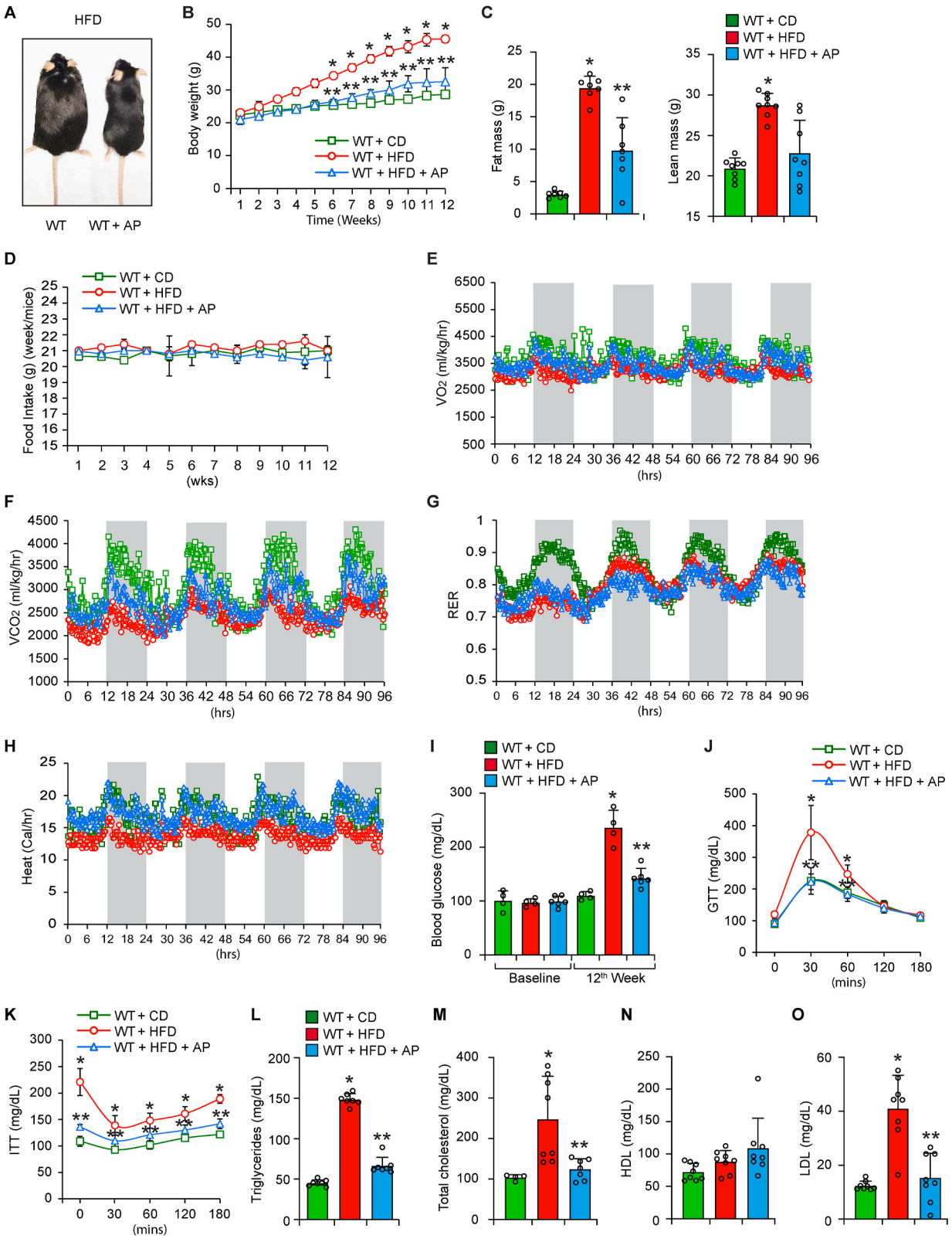

Fig. 5. Allopurinol prevents HFD-induced weight gain: A, Physical appearance of WT mice after 12 wks on HFD with or without Allopurinol. B, Changes in body weight of WT mice fed CD or HFD in combination with and without Allopurinol (125 mg/L of drinking water) for the indicated time periods (n = 7 in each group). C, Fat mass and lean mass of WT mice on the indicated diet for 12 wks. D, Food intake per day at the indicated time intervals by WT mice fed with the indicated diet (n = 6 in each group). E-H, O_2 consumption (E), CO_2 production (F), respiratory exchange ratio (G) and heat generation (H) levels in WT mice fed with CD or HFD in combination with and without Allopurinol for 12 wks (n = 8 in each group). I, Blood glucose levels in WT mice at day 1 and after 12 wks on the indicated diet. J and K, glucose tolerance (J) and insulin tolerance (K) of WT mice after 12 wks on the indicated diet (n = 7 in each group). L-O, Plasma TG (L), total cholesterol (M), HDL (N), and LDL (O) levels of WT mice on the indicated diet for 12 wks *, $p < 0.05$ versus WT mice on CD; **, $p < 0.05$ versus WT mice on HFD.

while DGAT2 knockout mice die soon after birth due to lipopenia [62], suggesting its essential role in TG biosynthesis. Our results showed that DGAT2 expression increases in the WAT of WT mice but not 12/15-LOX$^{-/-}$ mice on HFD. In addition, 12(S)-HETE, the arachidonic acid metabolite of 12/15-LOX, increases DGAT2 expression in 3T3-L1 adipocytes via p38MAPK-CREB-Egr1 signaling. HFD also activated p38MAPK-CREB-Egr1 signaling. These observations indicate that HFD via 12/15-LOX-mediated 12(S)-HETE production activates p38MAPK-CREB-Egr1 signaling leading to DGAT2 expression and WAT expansion. We have previously reported that LPS and cholesterol crystals via generation of H_2O_2 inhibit PP2A leading to activation of NFκB and affecting endothelial cell function [63,64]. To this end, the present

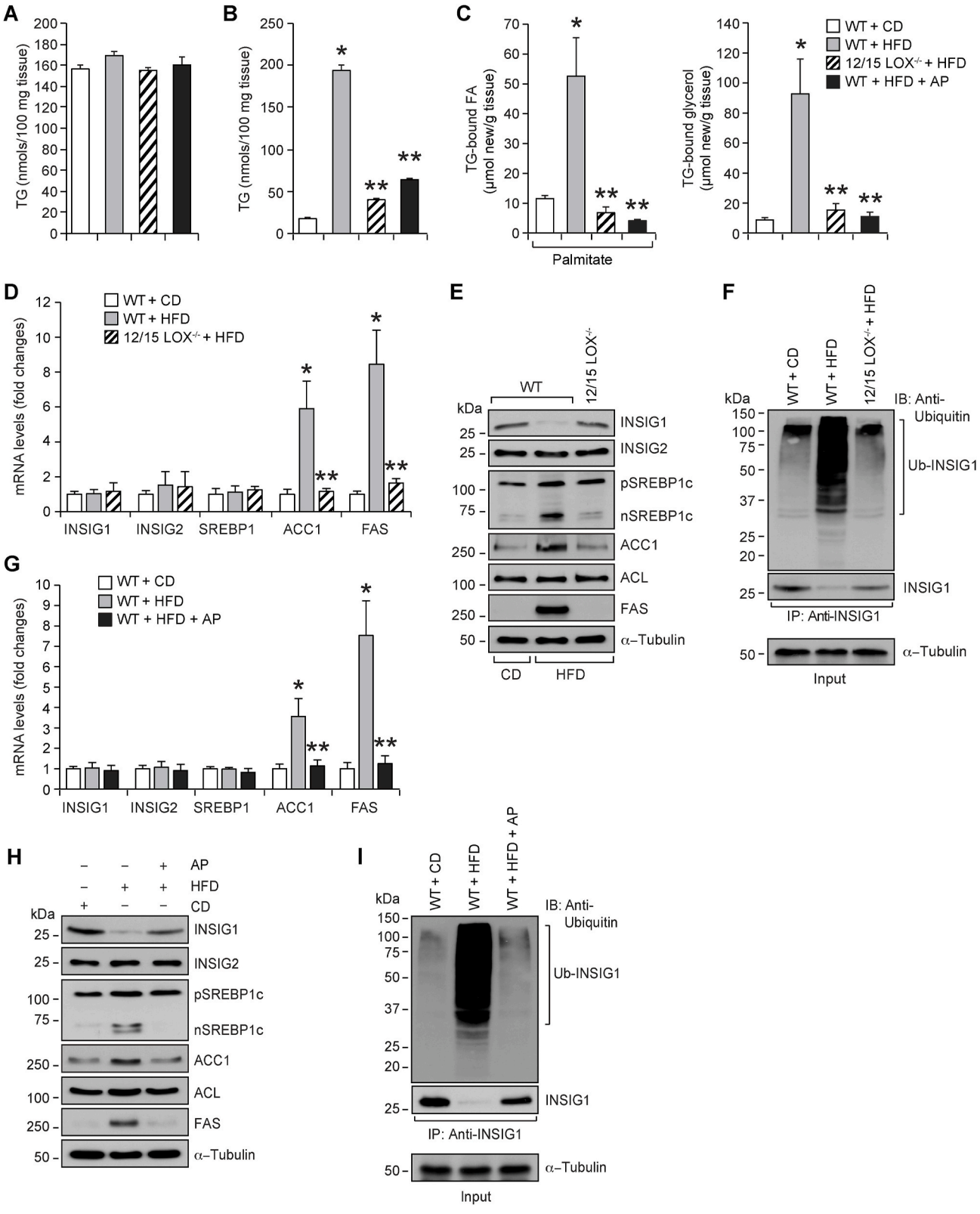

(caption on next page)

Fig. 6. 12/15-LOX mediates hepatic DNL and TG biosynthesis via INSIG1 ubiquitination, activation of SREBP1c and induction of ACC1 and FAS expression in XO dependent manner: A and B, WAT (A) and liver (B) extracts from WT and 12/15-LOX$^{-/-}$ mice fed with the indicated diet for 12 wks were analyzed for TG levels using Triglyceride Assay kit (Abcam). C, Mice fed with CD or HFD in combination with and without Allopurinol (12 wks) were fasted and given a bolus of $^{2}H_2O$ (ip) 5 h prior to tissue collection. Liver lipids were extracted and fractionated by GC-MS. Hepatic DNL was assessed as TG-bound ^{2}H-labeled fatty acid (palmitate) and hepatic TG biosynthesis was measured as TG-bound ^{2}H-labeled glycerol. D and E, Liver extracts of WT and 12/15-LOX$^{-/-}$ mice fed with CD or HFD (12 wks) were analyzed by qRT-PCR (D) and western blotting (E) for the indicated molecules using their specific primers and antibodies, respectively. F, Liver extracts of WT and 12/15-LOX$^{-/-}$ mice fed with CD of HFD (12 wks) were immunoprecipitated with INSIG1 antibody and the immunocomplexes were analyzed by western blotting using anti-ubiquitin antibody and the blots were probed for INSIG1. The same tissue extracts were analyzed by western blotting for α-tubulin. G and H, All the conditions were the same as in panels C and D except that liver extracts from WT mice fed with CD of HFD in combination with and without Allopurinol for 12 wks were analyzed by qRT-PCR (G) and western blotting (H) for the indicated molecules. I, All the conditions were the same as in panel E except that liver extracts from WT mice fed with CD of HFD in combination with and without Allopurinol for 12 wks were analyzed for INSIG1 ubiquitination. *, $p < 0.05$ versus WT mice on CD; **, $p < 0.05$ versus WT mice on HFD. AP, Allopurinol.

observations show that HFD induces the expression of XO leading to H_2O_2 production in WT mice but not in 12/15-LOX$^{-/-}$ mice. Furthermore, inhibition of XO by AP prevented HFD-induced p38MAPK-CREB-Egr1 signaling activation and DGAT2 expression leading to decreased fat mass and weight gain. These observations may reveal that 12/15-LOX via XO-mediated H_2O_2 production and p38MAPK-CREB-Egr1 signaling activation enhances DGAT2 expression, fat mass expansion and weight gain. These results were also consistent with the observations that inhibition of XO by AP restores the physical activity of these mice and this in turn may explain increased heat production by these mice. It is interesting to note that although XO expression at mRNA levels was induced both in WT and 12/15-LOX$^{-/-}$ mice, XO at protein levels was only upregulated in WT mice but not 12/15-LOX$^{-/-}$ mice. In fact, XO was found to be ubiquitinated in 12/15-LOX$^{-/-}$ mice by cullin2 and degraded. Based on these observations, it is likely that 12/15-LOX/12(S)-HETE axis is involved in the stabilization of XO and thereby promoting H_2O_2 production in the activation of p38MAPK-CREB-Egr1 signaling leading to DGAT2 expression, WAT expansion and weight gain. Many reports showed that H_2O_2 activates p38MAPK and CREB as well as several cellular signaling events [65–67], supporting its role in HFD-induced oxidative signaling leading to WAT expansion. Indeed, increased XO expression has also been reported in obese patients [68,69]. In contrast to these observations, a recent study has shown that either hepatocyte-specific deletion of XO or whole-body inhibition of XO by febuxostat while reducing systemic hyperuricemia had no effects on HFD-induced metabolic abnormalities such as insulin resistance and body weight gain [70]. However, another study has shown that whereas both XO inhibitors, namely allopurinol and febuxostat reduce blood uric acid levels, only febuxostat but not allopurinol reduce hepatic XO activity, UA levels and insulin resistance in a nonalcoholic steatohepatitis mouse model [71].

Although DGAT2 expression and WAT expansion were increased, the TG levels were not affected in WAT between WT and 12/15-LOX$^{-/-}$ mice. These observations imply that the increased WAT expansion might reflect esterification of fatty acids into TG in WAT and that these fatty acids are transported from the liver or absorbed from food. In this regard, our findings showed that HFD induces hepatic TG levels manyfold in WT mice as compared to 12/15-LOX$^{-/-}$ mice or WT mice treated with AP, suggesting increased TG synthesis in the liver. In fact, increased hepatic DNL and TG biosynthesis using $^{2}H_2O$ labeling in WT mice as compared to 12/15-LOX$^{-/-}$ mice or WT mice treated with AP on HFD support this view. In exploring the mechanisms by which 12/15-LOX plays a role in increased DNL, our results reveal that while HFD induces ubiquitination and degradation of INSIG1 leading to activation of SREBP1c and induction of its target genes ACC1 and FAS, these effects were suppressed in 12/15-LOX$^{-/-}$ mice. Our results also showed that HFD-induced INSIG1 ubiquitination/degradation, SREBP1c activation and ACC1 and FAS expression were sensitive to inhibition of XO by AP. SREBP1c plays an important role in hepatic DNL [72,73]. Based on these observations, we assume that 12/15-LOX via ubiquitination/degradation of INSIG1, activation of SREBP1c and induction of its target genes ACC1 and FAS expression plays a critical role in HFD-induced hepatic DNL. DGAT2 plays an essential role in TG biosynthesis [62], and our data showed an involvement of p38MAPK-CREB-Egr1 signaling in HFD-induced DGAT2 expression in WAT. Consistent with this view, we found that XO-p38MAPK-CREB-Egr1 signaling downstream to 12/15-LOX/12(S)-HETE axis plays a role in HFD-induced hepatic DGAT2 expression leading to TG biosynthesis. Furthermore, our results reveled that HFD induces VLDL structural protein ApoB100 [54] expression at both mRNA and protein levels in WT mice but not in 12/15-LOX$^{-/-}$ mice in a manner that is also sensitive to inhibition of XO. HFD-induced expression of SREBP1 and ApoB100 has recently been reported in mice [74]. Besides, it was also reported that dysregulation of VLDL production and secretion contributes to the pathogenesis of steatohepatitis [75]. The increased plasma TG levels in HFD-fed WT as compared to 12/15-LOX$^{-/-}$ mice were also reflected by increased TG biosynthesis along with increased ApoB100 expression in the liver and its enhanced rate of transport from the liver to AT for lipid esterification and storage.

XO converts hypoxanthine to xanthine and xanthine to uric acid with production of H_2O_2 as a metabolic byproduct [50] and the role of uric acid on hepatic DNL and TG biosynthesis has well been studied [76–78]. Although our results showed a role for XO in hepatic DNL and TG synthesis downstream to 12/15-LOX/12(S)-HETE axis, these observations do not clarify whether uric acid or H_2O_2 are involved in the modulation of these effects. To this end, our results show that H_2O_2 but not uric acid trigger ubiquitination/degradation of INSIG1, activation of SREBP1c and induction of its target genes ACC1 and FAS expression as well as activation of p38MAPK-CREB-Egr1 signaling and DGAT2 expression in hepatocytes. Based on these observations, it is likely that H_2O_2 mediated both hepatic DNL and TG biosynthesis downstream to 12/15-LOX/12(S)-HETE axis. H_2O_2 has been shown to play a role in lipid synthesis and its accumulation in hepatocytes [79,80], inhibition of lipolysis [81] and glycogen synthesis in adipocytes [82]. However, nothing is known about the role of H_2O_2 in weight gain. In summary, as shown in Fig. 9, it appears that H_2O_2 production downstream to 12/15-LOX mediates hepatic DNL via INSIG1 ubiquitination/degradation, SREBP1c activation and ACC1 and FAS expression; hepatic TG biosynthesis via activation of p38MAPK-CREB-Egr1 signaling and DGAT2 expression; and TG transport from liver to AT via expression of VLDL structural protein, ApoB100, for esterification and storage leading to WAT expansion and weight gain.

4. Materials and methods

4.1. Reagents

Anti-β-actin (sc-47778), anti-cullin1 (sc-17775), anti-DGAT1 (sc-26173), anti-Egr1 (sc-515830), anti-GFP (sc-9996), anti-INSIG1 (sc-390504), anti-PEPCK (sc-32879), anti-α-tubulin (sc-23948), anti-WT1 (sc-7385), and anti-XO (sc-398548) antibodies were bought from Santa Cruz Biotechnology (Santa Cruz, CA). Anti-CPT1B (ab104662), anti-cullin2 (ab166917), anti-cullin3 (ab75851), anti-INSIG2 (ab86415), anti-15-Lox1 (ab244205), and anti-SREBP1c (ab28481) antibodies, HDL and LDL/VLDL cholesterol assay kit (ab65390) and triglyceride quantification assay kit (ab65336) were obtained from Abcam

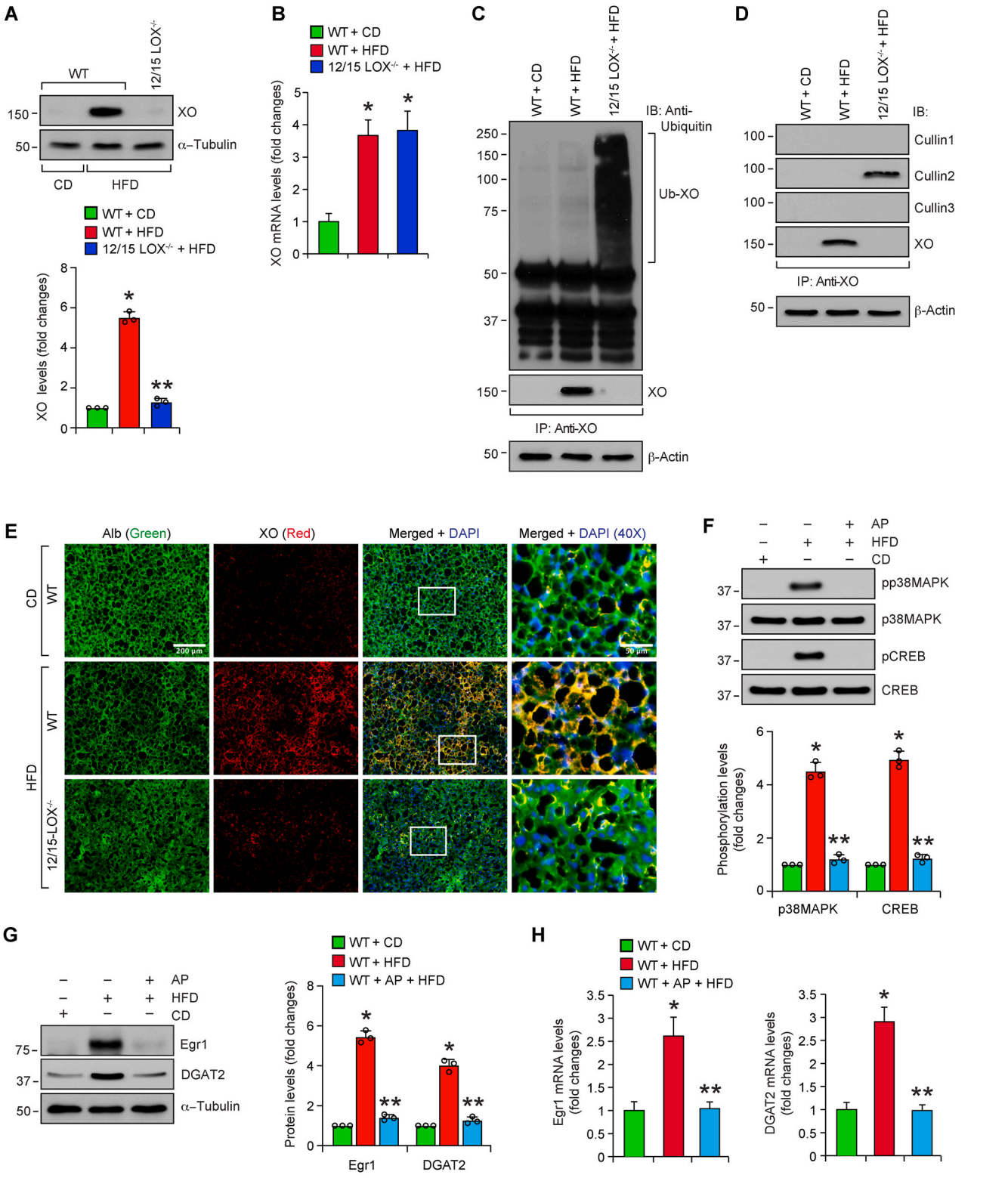

Fig. 7. 12/15-LOX deficiency leads to HFD-induced XO ubiquitination and degradation and Allopurinol mimics 12/15-LOX deficiency by inhibiting HFD-induced XO-mediated p38MAPK-CREB-Egr1 activation and DGAT2 expression in the liver: A and B, WT and 12/15-LOX$^{-/-}$ mice were fed with CD or HFD for 12 wks, and protein (A) and mRNA (B) levels of XO in the liver tissue were measured by western blotting and qRT-PCR, respectively. C and D, Liver extracts containing equal amounts of protein from each regimen were immunoprecipitated with anti-XO antibody and the immunocomplexes were analyzed by western blotting for the indicated proteins using their specific antibodies. The blots were reprobed for XO. The same tissue extracts were also analyzed by western blotting for β-actin. E, Liver sections of CD-fed WT mice and 12 wks of HFD-fed WT and 12/15-LOX$^{-/-}$ mice were coimmunostained for Albumin and XO. The selected areas in the 3rd column are shown in the 4th column at 40X magnification. F, WT mice were fed with CD or HFD in combination with and without Allopurinol (125 mg/L of drinking water) for 12 wks, and phosphorylation of p38MAPK and CREB were analyzed by western blotting in the liver and the blots were normalized for their total levels. G and H, The protein and RNA from the liver tissue of the mice in panel F were analyzed for Egr1 and DGAT2 protein and mRNA levels by western blotting (G) and qRT-PCR (H), respectively. *, $p < 0.05$ versus WT mice on CD; **, $p < 0.05$ versus WT mice on HFD.

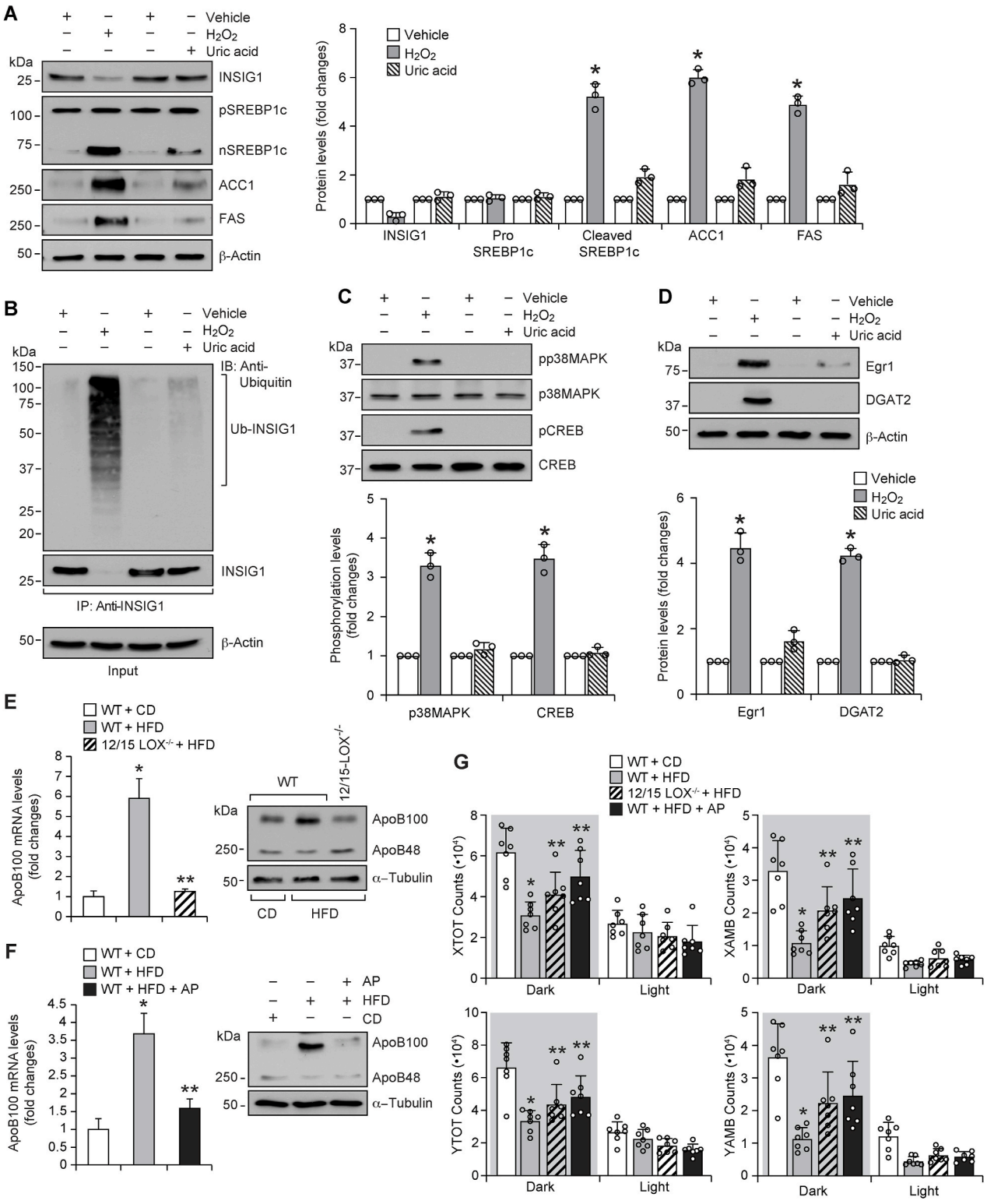

Fig. 8. H_2O_2 but not uric acid regulates HFD-induced 12/15-LOX-mediated hepatic DNL and TG biosynthesis: A, Mouse hepatocytes were growth-arrested, treated with vehicle or H_2O_2 (200 μM) or uric acid (100 μM) for 1 h and cell extracts were prepared and analyzed by western blotting for the indicated proteins using their specific antibodies. B, Cell extracts in panel A were immunoprecipitated with INSIG1 antibody and the immunocomplexes were analyzed by western blotting using anti-ubiquitin antibody and the blot was reprobed for INSIG1. The same cell extracts were analyzed by western blotting for β-actin. C and D, Cell extracts in panel A were analyzed by western blotting for the indicated proteins using their specific antibodies. E and F, Liver RNA and protein extracts of WT and 12/15-LOX$^{-/-}$ mice fed with CD or HFD for 12 wks (E) or WT mice fed with CD or HFD in combination with and without Allopurinol for 12 wks (F) were analyzed by qRT-PCR (left panels) and western blotting (right panels) for ApoB100. G, Spontaneous physical activity of mice with the indicated diet was measured over a 24-h period and shown as averaged counts of XTOT, XAMB, YTOT, and YAMB. Results were averaged separately over the light and dark cycles. The measurement was performed during the 6th week of HFD feeding (n = 8 in each group). *, $p < 0.05$ versus vehicle or WT mice on CD; **, $p < 0.05$ versus WT mice on HFD. AP, Allopurinol.

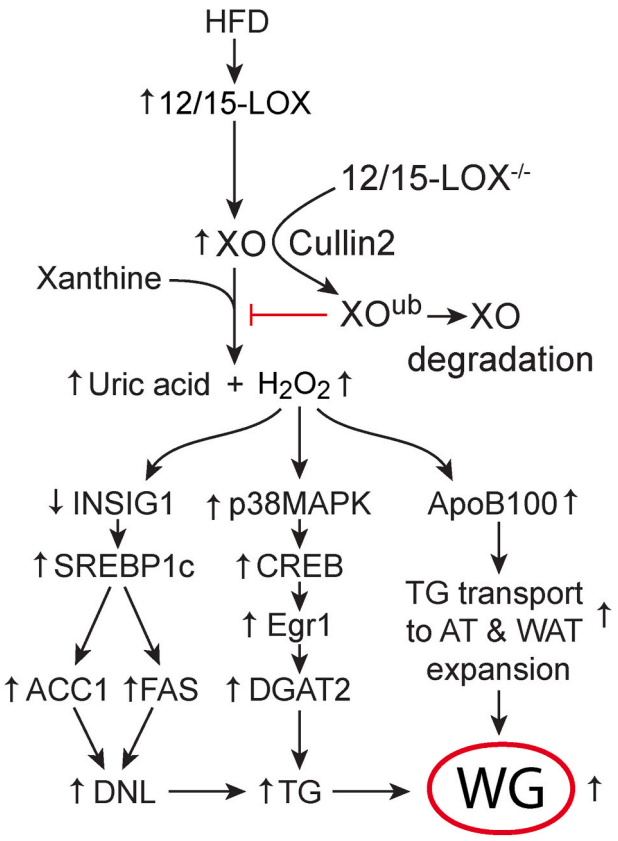

Fig. 9. Schematic diagram depicting the potential signaling events activated by 12/15-LOX/12(S)-HETE axis in response to HFD feeding leading to DNL and TG biosynthesis and promoting weight gain in mice.

(Cambridge, MA). Anti-ACC1 (3662S), anti-ACL (13390S), anti-AMPK (2532S), anti-pAMPK (2531S), anti-CREB (9197S), anti-pCREB (9198S), anti-FAS (3180S), anti-p38MAPK (8690S), anti-pp38MAPK (9215S), anti-mTOR (2972S), and anti-pmTOR (2971S) antibodies, and HRP-conjugated light chain specific anti-mouse (58802S) and anti-rabbit (93702S) IgGs were procured from Cell Signaling Technology (Beverly, MA). Anti-ubiquitin (P4D1) antibody was purchased from Enzo Life Sciences (Farmingdale, NY). Allopurinol (PHR1377), H_2O_2 (H1009), SB203580 (S8307), and uric acid (U2875) were bought from Sigma Aldrich Company (St Louis, MO). 12(*S*)-HETE (34570) was obtained from Cayman Chemical Company (Ann Arbor, MI). pGL3 basic vector, luciferase assay system (E4530) and PCR Master Mix (M750B) were purchased from Promega (Madison, WI). Thioglycollate medium brewer-modified (21176) was obtained from BD Biosciences (San Jose, CA). Control non-targeting siRNA (D-001810-10) was obtained from Dharmacon RNAi Technologies (Chicago, IL). Mouse CREB Silencer Select (ID-XX) was purchased from Ambion (Waltham, MA). Horseradish peroxidase (HRP)-conjugated goat anti-rabbit IgG (31460) and goat anti-mouse IgG (31437), anti-DGAT2 antibody (PA5-18667), Amplex Red Hydrogen Peroxide Assay kit (A22188), Quickchange Lightning Site-Directed Mutagenesis kit (210518–5), Biotin 3′-end DNA labeling kit (89818) and light-shift chemiluminescent electrophoretic mobility shift assay (EMSA) kit (20148), One Shot TOP10 Chemically Competent *Escherichia coli* (C404003), and Lipofectamine 3000 transfection reagent (L3000-015) were obtained from Thermo Fisher Scientific (Waltham, MA). Enhanced chemiluminescence Western blotting detection reagents (RPN2106) were purchased from GE Healthcare (Pittsburg, PA). Quick Ligation Kit (M2200S) was bought from New England Biolabs (Ipswich, MA). All the primers used for qRT-PCR (quantitative reverse transcription polymerase chain reaction), cloning, site-directed mutagenesis, and EMSA were synthesized by IDT (Coralville, IA) and listed in Table 1.

4.2. Animals

Both male and female 12/15-LOX$^{-/-}$ mice (B6·129S2-*Alox15*^{tm1Fun}/J; Stock #002778) and C57BL/6J (Stock #000664) mice were purchased from The Jackson Laboratory (Bar Harbor, ME) and Charles River Laboratories (Wilmington, MA), respectively, and maintained at the University of Tennessee Health Science Center's animal facilities. The UTHSC LACU facility maintains a 12/12 h light/dark cycle and the animals have ad libitum access to food and water. Mice were bred and maintained according to the institutional animal facility guidelines. All the experiments involving the use of animals have been approved by the Animal Care and Use Committee of the University of Tennessee Health Science Center, Memphis, TN. To study diet-induced weight gain, 8-week-old mice were placed on control chow diet (CD) or high-fat diet (HFD) containing 21.2% fat, 0.2% cholesterol, 48.5% carbohydrate, and 17.3% protein (TD88137, Harlan Teklad, Madison, MI) in combination with and without Allopurinol (125 mg/L of drinking water) for the indicated time period. At the end of the experimental period, mice ware sacrificed by ketamine/xylazine overdose and blood, liver and adipose tissue were collected for further analysis as required. All 12/15-LOX$^{-/-}$ mice used in this study were genotyped using DNA isolated from tail biopsy and the following primers: common forward, 5′-GGC TGC CTG AAG AGG TAC AG-3'; wild type reverse, 5′-CCA TAG ACG AGA CCA GCA CA-3'; and mutant reverse, 5′-GGG AGG ATT GGG AAG ACA AT-3'.

4.3. Adipocyte size

After feeding with the indicated diet for 12 wks, mice were euthanized with ketamine (100 mg/kg BW)/xylazine (15 mg/kg BW), adipose tissue was dissected out, fixed in 4% paraformaldehyde overnight, washed with PBS and blocks were prepared in OCT. AT cryosections were made on Leica CM3050S Cryostat (Leica Biosystems Inc., Buffalo Grove, IL) and stained with H&E. Sections were observed under Nikon Eclipse TS100 (10X/0.25NA) and images were captured with Nikon DS-Fi2 connected with Nikon Microscope Camera Control Unit DS-L3. Adipocyte size was measured and quantified according to the method described by Parlee et al. [83], using ImageJ V 1.53a software.

4.4. Metabolic studies

Eight-weeks old C57BL/6J and 12/15-LOX$^{-/-}$ mice were placed on CD or HFD (42% calories from fat, 15.3% calories from protein and 42.7% calories from carbohydrate, primarily sucrose; TD#88137; Harlan Teklad, Madison, WI) and monitored over a period of 12 wks. Body weight and food intake were measured weekly. The EchoMRI_1100 (quantitative magnetic resonance) was used to measure body composition (total fat and lean mass and total and free body water) prior to measurements of total energy expenditure. Indirect calorimetry was performed on mice individually housed in a home cage style Comprehensive Laboratory Animal Monitoring System (CLAMS; Columbus Instruments, Columbus, OH) [84]. Metabolic parameters for each mouse were measured over a 6 day period post 1 day acclimation at 22 °C. Oxygen consumption (VO_2; ml/h) and carbon dioxide production (VCO_2; ml/h) were determined by open-circuit indirect calorimetry using Oxymax software. Total energy expenditure was determined as HEAT. The respiratory exchange ratio (RER) was calculated as the ratio of VCO_2 to VO_2. Infrared beam interruptions on both X-axis (horizontal) and Y-axis (vertical) were measured to quantify the spontaneous physical activity of mice in both the directions. Total beam breaks on X-axis (XTOT) and total beam breaks on Y-axis (YTOT) were summed to provide total horizontal activity and total vertical activity, respectively. Two or more consecutive beam breaks on X-axis (horizontal) and on Y-axis (vertical) were recorded as ambulatory activity on X-axis (XAMB) and ambulatory activity on Y-axis (YAMB), respectively.

Table 1
List of primers used in this study.

Primers	Forward primer 5′ → 3′	Reverse primer 5′ → 3′
qRT-PCR		
Mouse DGAT2	CTCTCAGCCCTCCAAGACAT	GGTGAAGTAGAGCACAGCTATCAG
Mouse Egr1	CAGAAGGACAAGAAAGCAGACA	AGCCAGGAGAGGAGTAGGAAG
Mouse XO	AAGACGTTGCGTTTTGAAGG	GGGCAGATGATCAGAGGAAAT
Mouse INSIG1	ACCTGGGAGAACCACACAAG	CTTCGGGAACGATCAAATGT
Mouse INSIG2	CGGGGTGGTACTCTTCTTCA	GGGTACAACAGCCCAATCAC
Mouse SREBP1	CACTCAGCAGCCACCATCTA	AGGTACTGTGGCCAAGATGG
Mouse ACC1	GCCTCTTCCTGACAAACGAG	TGACTGCCGAAACATCTCTG
Mouse FAS	TGGGTTCTAGCCAGCAGAGT	ACCACCAGAGACCGTTATGC
DGAT2 promoter cloning		
mDGAT2p	ATAAGGTACCACAAGAACATGGCACAGTCC	CGCTAAGCTTGCAGATCCTTTATTCTTGTTTTCG
Site-directed mutagenesis		
mDGAT2p-CREB-Mt	GCTTTCTGCACGGCCGTTTTGTGCATTGGCTTCAGC	GCTGAAGCCAATGCACAAAACGGCCGTGCAGAAAGC
mDGAT2p-Egr1-Mt	TGCTGCCGCCACGGCCAAAGCGCTGTCCCTCAG	CTGAGGGACAGCGCTTTGGCCGTGGCGGCAGCA
EMSA		
mDGAT2p-CREB-Wt	GCTTTCTGCACGGCCGTGACGTGCATTGGCTTCAGC	GCTGAAGCCAATGCACGTCACGGCCGTGCAGAAAGC
mDGAT2p-CREB-Mt	GCTTTCTGCACGGCCGTTTTGTGCATTGGCTTCAGC	GCTGAAGCCAATGCACAAAACGGCCGTGCAGAAAGC
mDGAT2p-Egr1-Wt	TGCTGCCGCCACGGCCTGGGCGCTGTCCCTCAG	CTGAGGGACAGCGCCCAGGCCGTGGCGGCAGCA
mDGAT2p-Egr1-Mt	TGCTGCCGCCACGGCCAAAGCGCTGTCCCTCAG	CTGAGGGACAGCGCTTTGGCCGTGGCGGCAGCA

4.5. De novo lipogenesis and triglyceride biosynthesis in vivo using heavy water (^2H_2O) method

Measurements of DNL and newly made TG's and their respective contents were determined following a bolus of ^2H_2O saline via intraperitoneal administration to the mice (30 μl of ^2H_2O per g body weight in saline; 99% purity). Mice were allowed to sit in their cages for 5 h prior to tissue collection. Blood and tissue samples are collected and flash-frozen in liquid nitrogen and stored until gas chromatography-mass spectrometry (GC-MS) analysis was performed. Triglycerides from livers were isolated using organic solvent extraction method, and the ^{2}H-labeled glycerol and palmitate were analyzed by GC-MS after derivatization. The ^{2}H-labeled triglyceride covalently linked to palmitate and glycerol measures the amount of newly synthesized palmitate and triglyceride, respectively. The ^2H_2O contribution of de novo lipogenesis to the pool of FA (palmitate) and triglycerides (glycerol) was then calculated according to previously described methods [85,86]. Briefly, DNL reflects the newly made palmitate pool which was based on the measured total contents (μmol/g tissue) and percent ^{2}H-labeled palmitate as a function of percent ^{2}H-labeled body water. Similarly, the total newly made triglyceride pool was based % total newly made triglyceride-bound glycerol (^{2}H-labeled triglyceride-glycerol) and total glycerol content. Isotopic enrichments of body water and contents of TG-bound fatty acids and glycerol were determined using a mass selective detector equipped with a gas chromatography mass spectrometry system (Agilent 7000C Triple Quadrupole GC-MS system (Agilent Technologies, Santa Clara, CA).

4.6. GTT & ITT

After feeding with the indicated diet for 12 wks along with and without allopurinol (125 mg/L of drinking water), glucose tolerance test (GTT) and insulin tolerance test (ITT) were performed in mice after 6 h of fasting. For both GTT and ITT, first baseline blood glucose concentration was measured from tail tip blood samples using OneTouch Verio glucometer (Malvern, PA). GTT was performed by injecting fresh glucose solution intraperitoneally (2 g/kg BW) and measuring blood glucose levels at 30, 60, 120 and 180 min after glucose injection. For ITT, insulin (Cat # 91077C from Sigma-Aldrich) was injected intraperitoneally (1 IU/kg BW) and blood glucose levels were measured at 30, 60, 120 and 180 min after insulin injection.

4.7. Plasma lipid profiles

Blood was collected into BD Vacutainer Plus plasma tubes (Cat # 367960, BD Biosciences) by cardiac puncture and centrifuged at 1,300g for 10 min at 4 °C to collect the plasma. Total plasma cholesterol, HDL, LDL, and TG levels were measured by using HDL and LDL/VLDL cholesterol assay kit (ab65390) and triglyceride quantification assay kit (ab65336), following the manufacturer's instructions.

4.8. H_2O_2 production assay

Tissue lysates were incubated with 50 μl of 100 μM Amplex Red along with 0.2 U/ml of HRP for 30 min at 37 °C in the dark. Following incubation, the fluorescence intensity was measured in SpectraMax Gemini XPS Spectrofluorometer (Molecular Devices) with excitation at 530 nm and emission at 590 nm. The H_2O_2 production was expressed as RFU.

4.9. Cell culture

3T3-L1 mouse embryonic fibroblasts were obtained from ATCC (Cat # CL-173) and sub-cultured in DMEM supplemented with 10% bovine calf serum for pre-adipocyte expansion. To obtain fully differentiated adipocytes, pre-adipocytes were supplemented with dexamethasone (1 μM), methylisobutylxanthine (0.5 mM) and insulin (1 μg/ml) along with bovine calf serum in DMEM following the manufacturer's instructions. Mouse hepatocytes were purchased from Thermo Fisher Scientific (Cat #MSCP10), and sub-cultured in William's E Medium (no phenol red) supplemented with primary hepatocyte thawing and plating supplements. Cell cultures were maintained in a humidified 95% air and 5% CO_2 atmosphere at 37 °C. Cells were growth-arrested overnight in medium without any growth supplements and used for the experiments unless otherwise indicated.

4.10. Transfections

Differentiated 3T3-L1 adipocytes were transfected with scrambled or targeted siRNA at a final concentration of 100 nmoles using Lipofectamine 3000 transfection reagent according to the manufacturer's instructions. Wherever plasmid vectors were used, differentiated 3T3-L1 adipocytes were transfected with plasmid DNAs at a final concentration of 2.5 μg/60 mm culture dish or 5 μg/100 mm culture dish using Lipofectamine 3000 transfection reagent. After transfections, cells were recovered in complete medium for 24 h, quiesced overnight in serum-

free medium and used as needed.

4.11. Adenoviral vectors

Construction of Ad-GFP, Ad-Egr1 and Ad-KCREB were described previously [43,87,88]. The adenovirus was purified by cesium chloride gradient ultracentrifugation [89]. Wherever adenoviral vectors were used to block the function of CREB or Egr1, cells were infected with adenovirus harboring GFP or dominant negative mutant of the target molecule at 40 moi overnight in complete medium. After infections, cells were growth-arrested for 48 h and used as required.

4.12. Quantitative RT-PCR

Total cellular RNA was isolated from mouse hepatocytes, 3T3-L1 cells, adipose tissue and liver using TRIzol reagent as per the manufacturer's instructions. Reverse transcription was performed with a high-capacity complementary DNA reverse transcription kit (Applied Biosystems, Foster City, CA). Quantitative reverse transcriptase-PCR was then performed on a 7300 Real-Time PCR system (Applied Biosystems) using SYBR Green Master Mix (Applied Biosystems) as per the manufacturer's instructions. Beta actin was used as the endogenous control. The PCR amplifications were examined using the 7300 Real-Time PCR system operated SDS version 1.4 program and Delta Rn analysis method (Applied Biosystems). The primers used for quantitative reverse transcriptase-PCR are shown in Table 1.

4.13. Western blotting

After the indicated treatments, cells were scraped into RIPA buffer (PBS containing 1% Nonidet P40, 0.5% sodium deoxycholate, 0.1% SDS, 100 μg/ml PMSF, 100 μg/ml aprotinin, 1 μg/ml leupeptin, and 1 mM sodium orthovanadate) and lysed by sonication at 45% amplitude for 15 s with 10 s intervals for 2 min on ice (Branson Sonifier 450). To prepare liver extracts, it was minced in RIPA buffer and homogenized by sonication at 45% amplitude for 15 s with 10 s intervals for 4 min on ice. To prepare adipose tissue extract, it was minced and homogenized in 50 mM HEPES buffer (pH 7.5) containing 100 mM NaCl, 10% SDS, 2 mM EDTA, 0.5 mM DTT, 1 mM Benzamidine, 100 μg/ml PMSF, 100 μg/ml aprotinin, 1 μg/ml leupeptin, and 1 mM sodium orthovanadate at tissue to homogenization buffer ratio of 1:2 (i.e., 300 mg tissue in 600 μl homogenization buffer) using Miltenyi Biotec gentleMACS Octo Dissociator and centrifuged. The infranatant was carefully collected without mixing upper fat cake layer. The collected infranatant was re-centrifuged four times to remove fat debris completely. Cell or tissue extracts were cleared by centrifugation at 12,000 rpm for 10 min at 4 °C and protein concentration was determined using Mico BCA kit (Thermo Scientific). Cell or tissue extracts containing equal amounts of protein (40 μg) from each regimen were resolved by electrophoresis on 0.1% (w/v) SDS and 8% or 10% (w/v) polyacrylamide gels. The proteins were transferred electrophoretically onto nitrocellulose membranes. After blocking in 5% (w/v) non-fat dry milk or 5% BSA, the membranes were incubated with appropriate primary antibodies at 1:1000 dilution overnight at 4 °C followed by incubation with horseradish peroxidase-conjugated secondary antibodies at 1:5000 dilution for 1 h at RT. The membranes were washed three times with Tris buffered saline (TBS) containing Tween 20 and once with TBS alone. The antigen-antibody complexes were detected using enhanced chemiluminescence detection reagent kit (GE Healthcare). The band intensities were quantified by densitometry using NIH ImageJ V 1.53a software.

4.14. Immunoprecipitation

Cell or tissue extracts were prepared by lysis in 400 μl of lysis buffer (PBS, 1% Nonidet P40, 0.5% sodium deoxycholate, 0.1% SDS, 100 μg/ml PMSF, 100 μg/ml aprotinin, 1 μg/ml leupeptin, and 1 mM sodium orthovanadate) for 20 min on ice. The extracts were cleared by centrifugation at 12000 rpm for 15 min at 4 °C. The cleared extracts containing an equal amount of protein (400 μg) from control and the indicated treatments was incubated with the indicated antibodies (4 μg) overnight at 4 °C, followed by incubation with protein A/G-Sepharose CL4B beads (80 μl of 50% w/v slurry) for 4 h with gentle rocking. The beads were collected by centrifugation at 1000 rpm for 2 min at 4 °C and washed four times with lysis buffer and once with PBS. The immunocomplexes were released by heating the beads in 40 μl of Laemmli sample buffer and analyzed by Western blotting for the indicated molecules using their specific antibodies.

4.15. Immunofluorescence staining

After feeding with the indicated diet for 12 wks, mice were anesthetized, perfused with PBS followed by 4% paraformaldehyde (PFA) and euthanized. Liver was harvested, fixed in OCT and 8 μm transverse sections were made on a Leica CM3050S cryostat. After permeabilization in 0.5% Triton X100 and blocking in normal goat serum, the sections were probed with mouse anti-XO antibody (1:50 dilution) in combination with rabbit anti-albumin antibody (1:100 dilution) followed by incubation with Alexa Fluor 568-conjugated goat anti-mouse (1:500 dilution) and Alexa Fluor 488-conjugated goat anti-rabbit secondary (1:500 dilution) antibodies. The sections were washed with PBS, mounted in ProLong Gold antifade reagent and observed under a Zeiss inverted microscope (Axiovision Observer.z1; 40X/NA 0.6 or 10X/NA 0.45). The fluorescence images were captured by a Zeiss AxioCam MRm camera using the microscope operating and image analysis software Zen 2.6 (blue edition) (Carl Zeiss Imaging Solutions GmbH).

4.16. Cloning

The mouse DGAT2 (mDGAT2) proximal promoter was cloned into pGL3 basic vector (Promega) to yield pGL3-mDGAT2p-Luc construct as per the methods described by us previously [90]. Briefly, mouse DGAT2 proximal promoter encompassing −312 to +92 nt relative to the transcription start site was amplified from mouse genomic DNA using forward primer (mDGAT2pF) incorporating a KpnI restriction site at the 5′ end and a reverse primer (mDGAT2pR) incorporating a HindIII restriction site at the 5′ end. The PCR product was digested with KpnI and HindIII, and the released fragment was cloned into KpnI and HindIII sites of pGL3 basic vector (Promega) to yield pGL3-mDGAT2p-Luc construct. Site-directed mutations within the CREB and Egr1 binding sites at −12 nt and −117 nt, respectively, were introduced by using the QuikChange Lightning site-directed mutagenesis kit following manufacturer's instructions. Plasmid DNAs were purified using the EndoFree plasmid maxi kit (Catalog #. 12362; Qiagen) and used for the transfections. The primers used for cloning and site-directed mutagenesis of mDGAT2 promoter are shown in Table 1.

4.17. Luciferase assay

Differentiated 3T3-L1 cells were transfected with pGL3 basic vector or pGL3-mDGAT2p construct with and without the indicated mutations using Lipofectamine 3000 transfection reagent for 6 h. After 24 h of recovery in complete medium, cells were growth-arrested in serum-free medium overnight. Cells were then treated with and without 12(S)-HETE (0.5 μM) for 2 h, washed with PBS, and lysed in 200 μl of lysis buffer. The cell extracts were cleared by centrifugation at 12,000 rpm for 2 min at 4 °C. The supernatants were assayed for luciferase activity using luciferase assay system (Promega) and a single tube luminometer (TD20/20; Turner Designs, Sunnyvale, CA). The values are expressed as relative luciferase units. In the case of adenoviral vectors, cells were infected with Ad-GFP or Ad-KCREB or Ad-Egr1 at 40 moi overnight in complete medium. After infections, cells were growth-arrested for 48 h and used as needed for luciferase assay.

4.18. EMSA

Nuclear extracts of differentiated 3T3-L1 cells with appropriate treatments were prepared using NE-PER nuclear and cytoplasmic extraction kit (Catalog #78833, Thermo Fisher Scientific) according to the manufacturer's protocol. The protein content of the nuclear extracts was determined using a micro-BCA method (Pierce Biotechnology). Double stranded oligonucleotides encompassing CREB binding element located at −12 nt, and Egr1 binding element located at −117 nt of mDGAT2 promoter were used as biotin-labeled probes (Table 1) to measure protein-DNA binding activity. Briefly, 5 μg of nuclear extract was incubated in a binding buffer (10 mM Tris-HCl, pH 7.5, 50 mM KCl, 1 mM DTT, 2.5% glycerol) with 5 nM of biotin-labeled probe and 1 μg of poly(dI-dC) for 30 min at room temperature in a total volume of 20 μl on ice, and the protein-DNA complexes were resolved by electrophoresis on a 6% polyacrylamide gel using Tris borate-EDTA buffer (44.5 mM Tris-HCl, 44.5 mM borate, and 20 mM EDTA, pH 8.0). After separation, the protein-DNA complexes were transferred to nylon membrane using Trisborate-EDTA buffer, UV cross-linked, and visualized by chem-iluminescence. To perform supershift EMSA, the complete reaction mix was incubated with 2 μg of the indicated antibody for 1 h on ice before separating it by electrophoresis. Normal serum was used as negative control.

4.19. Statistics

All the in vitro experiments were repeated 3 times. The treatment effects were analyzed by student *t*-test for two group comparisons and one-way analysis of variance (ANOVA) followed by Bonferroni post hoc test for multi group comparisons. In the case of in vivo experiments, a minimum of 12 mice were included in each group and the normality of the data (by D'Agostino-Pearson normality test) and equality of group variance (by *F* test) tests were performed using GraphPad Prism v 8.00 software. The normally distributed data with similar variance were then analyzed by one-way ANOVA followed by Tukey's post hoc test or two-tailed student *t*-test. Since we did not observe statistical differences between male and female mice in our experiments on weight gain, we did not express the results separately. The data are presented as Mean ± SD and the $p < 0.05$ were considered statistically significant.

Source of funding

HL074860 and HL103575.

Author contributions

S.G. conducted the experiments, analyzed the data, and wrote the manuscript. P.P., A.M.M., R.K., D.S., A.D., S.M., and M.A.P. conducted the experiments and analyzed the data. E.A.P. project discussions and helped in writing the manuscript. G.N.R., conceived the overall project, designed the experiments, interpreted the results, and corrected the manuscript.

Declaration of competing interest

None.

Acknowledgements

We are thankful to Dr. Nathan G. Tipton for editing the manuscript.

Appendix A. Supplementary data

Supplementary data to this article can be found online at https://doi.org/10.1016/j.redox.2021.102163.

References

[1] A. De Lorenzo, S. Gratteri, P. Gualtieri, A. Cammarano, P. Bertucci, L. Di Renzo, Why primary obesity is a disease? J. Transl. Med. 17 (2019) 169.
[2] D.W. Haslam, W.P. James, Obesity, Lancet 366 (2005) 1197–1209.
[3] X. Pi-Sunyer, The medical risks of obesity, Postgrad. Med. 121 (2009) 21–33.
[4] W.P.T. James, K. McPherson, The costs of overweight, Lancet Public Health 2 (2017) e203–e204.
[5] J. Kjellberg, A. Tange Larsen, R. Ibsen, B. Højgaard, The socioeconomic burden of obesity, Obes. Facts 10 (2017) 493–502.
[6] B.E. Wisse, F. Kim, M.W. Schwartz, Physiology. An integrative view of obesity, Science 318 (2007) 928–929.
[7] D.K. Patel, F.C. Stanford, Safety and tolerability of new-generation anti-obesity medications: a narrative review, Postgrad. Med. 130 (2018) 173–182.
[8] H. Kuhn, L. Humeniuk, N. Kozlov, S. Roigas, S. Adel, D. Heydeck, The evolutionary hypothesis of reaction specificity of mammalian ALOX15 orthologs, Prog. Lipid Res. 72 (2018) 55–74.
[9] N.K. Singh, G.N. Rao, Emerging role of 12/15-Lipoxygenase (ALOX15) in human pathologies, Prog. Lipid Res. 73 (2019) 28–45.
[10] A.D. Dobrian, D.C. Lieb, B.K. Cole, D.A. Taylor-Fishwick, S.K. Chakrabarti, J. L. Nadler, Functional and pathological roles of the 12- and 15-lipoxygenase, Prog. Lipid Res. 50 (2011) 115–131.
[11] H. Kuhn, M. Walther, R.J. Kuban, Mammalian arachidonate 15-lipoxygenases structure, function, and biological implications, Prostag. Other Lipid Mediat. 68–69 (2002) 263–290.
[12] X.S. Chen, U. Kurre, N.A. Jenkins, N.G. Copeland, C.D. Funk, cDNA cloning, expression, mutagenesis of C-terminal isoleucine, genomic structure, and chromosomal localizations of murine 12-lipoxygenases, J. Biol. Chem. 269 (1994) 13979–13987.
[13] D.J. Conrad, The arachidonate 12/15 lipoxygenases. A review of tissue expression and biologic function, Clin. Rev. Allergy Immunol. 17 (1999) 71–89.
[14] T. Cyrus, J.L. Witztum, D.J. Rader, R. Tangirala, S. Fazio, M.F. Linton, C.D. Funk, Disruption of the 12/15-lipoxygenase gene diminishes atherosclerosis in apo E-deficient mice, J. Clin. Invest. 103 (1999) 1597–1604.
[15] S. Kotla, N.K. Singh, M.R. Heckle, G.J. Tigyi, G.N. Rao, The transcription factor CREB enhances interleukin-17A production and inflammation in a mouse model of atherosclerosis, Sci. Signal. 6 (2013) ra83.
[16] H. Kühn, I. Römisch, J. Belkner, The role of lipoxygenase-isoforms in atherogenesis, Mol. Nutr. Food Res. 49 (2005) 1014–1029.
[17] M. Martínez-Clemente, N. Ferré, E. Titos, R. Horrillo, A. González-Périz, E. Morán-Salvador, C. López-Vicario, R. Miquel, V. Arroyo, C.D. Funk, J. Clària, Disruption of the 12/15-lipoxygenase gene (Alox15) protects hyperlipidemic mice from nonalcoholic fatty liver disease, Hepatology 52 (2010) 1980–1991.
[18] M. Lazic, M.E. Inzaugarat, D. Povero, I.C. Zhao, M. Chen, M. Nalbandian, Y. I. Miller, A.C. Cherñavsky, A.E. Feldstein, D.D. Sears, Reduced dietary omega-6 to omega-3 fatty acid ratio and 12/15-lipoxygenase deficiency are protective against chronic high fat diet-induced steatohepatitis, PLoS One 9 (2014), e107658.
[19] B.K. Cole, M.A. Morris, W.J. Grzesik, K.A. Leone, J.L. Nadler, Adipose tissue-specific deletion of 12/15-lipoxygenase protects mice from the consequences of a high-fat diet, Mediat. Inflamm. 2012 (2012) 851798.
[20] C.S. Nunemaker, M. Chen, H. Pei, S.D. Kimble, S.R. Keller, J.D. Carter, Z. Yang, K. M. Smith, R. Wu, M.H. Bevard, J.C. Garmey, J.L. Nadler, 12-Lipoxygenase-knockout mice are resistant to inflammatory effects of obesity induced by Western diet, Am. J. Physiol. Endocrinol. Metab. 295 (2008) E1065–E1075.
[21] D.D. Sears, P.D. Miles, J. Chapman, J.M. Ofrecio, F. Almazan, D. Thapar, Y. I. Miller, 12/15-lipoxygenase is required for the early onset of high fat diet-induced adipose tissue inflammation and insulin resistance in mice, PLoS One 4 (2009), e7250.
[22] Y. Guo, W. Zhang, C. Giroux, Y. Cai, P. Ekambaram, A.K. Dilly, A. Hsu, S. Zhou, K. R. Maddipati, J. Liu, S. Joshi, S.C. Tucker, M.J. Lee, K.V. Honn, Identification of the orphan G protein-coupled receptor GPR31 as a receptor for 12-(S)-hydroxyeicosatetraenoic acid, J. Biol. Chem. 286 (2011) 33832–33840.
[23] S.C. Burgess, T. He, Z. Yan, J. Lindner, A.D. Sherry, C.R. Malloy, J.D. Browning, M. A. Magnuson, Cytosolic phosphoenolpyruvate carboxykinase does not solely control the rate of hepatic gluconeogenesis in the intact mouse liver, Cell Metabol. 5 (2007) 313–320.
[24] R.W. Brownsey, A.N. Boone, J.E. Elliott, J.E. Kulpa, W.M. Lee, Regulation of acetyl-CoA carboxylase, Biochem. Soc. Trans. 34 (2006) 223–227.
[25] T. Kim, L. He, M.S. Johnson, Y. Li, L. Zeng, Y. Ding, Q. Long, J.F. Moore, J. D. Sharer, T.R. Nagy, M.E. Young, P.A. Wood, Q. Yang, Carnitine palmitoyltransferase 1b deficiency protects mice from diet-induced insulin resistance, J. Diabetes Metabol. 5 (2014) 361.
[26] H. Cai, L.Q. Dong, F. Liu, Recent advances in adipose mTOR signaling and function: therapeutic prospects, Trends Pharmacol. Sci. 37 (2016) 303–317.
[27] L. Khamzina, A. Veilleux, S. Bergeron, A. Marette, Increased activation of the mammalian target of rapamycin pathway in liver and skeletal muscle of obese rats: possible involvement in obesity-linked insulin resistance, Endocrinology 146 (2005) 1473–1481.
[28] L. Ma, S. Ma, H. He, D. Yang, X. Chen, Z. Luo, D. Liu, Z. Zhu, Perivascular fat-mediated vascular dysfunction and remodeling through the AMPK/mTOR pathway in high-fat diet-induced obese rats, Hypertens. Res. 33 (2010) 446–453.
[29] J. Xu, J. Ji, X.H. Yan, Cross-talk between AMPK and mTOR in regulating energy balance, Crit. Rev. Food Sci. Nutr. 52 (2012) 373–381.
[30] J. Kim, K.L. Guan, mTOR as a central hub of nutrient signalling and cell growth, Nat. Cell Biol. 21 (2019) 63–71.

[31] C.L. Lyons, H.M. Roche, Nutritional modulation of AMPK-impact upon metabolic-inflammation, Int. J. Mol. Sci. 19 (2018) 3092.
[32] A. González, M.N. Hall, S.C. Lin, D.G. Hardie, AMPK and TOR: the yin and yang of cellular nutrient sensing and growth control, Cell Metabol. 31 (2020) 472–492.
[33] S. Li, M.S. Brown, J.L. Goldstein, Bifurcation of insulin signaling pathway in rat liver: mTORC1 required for stimulation of lipogenesis, but not inhibition of gluconeogenesis, Proc. Natl. Acad. Sci. U.S.A. 107 (2010) 3441–3446.
[34] D.G. McLaren, S. Han, B.A. Murphy, L. Wilsie, S.J. Stout, H. Zhou, T.P. Roddy, J. N. Gorski, D.E. Metzger, M.K. Shin, D.F. Reilly, H.H. Zhou, M. Tadin-Strapps, S. R. Bartz, A.M. Cumiskey, T.H. Graham, D.M. Shen, K.O. Akinsanya, S.F. Previs, J. E. Imbriglio, S. Pinto, DGAT2 inhibition alters aspects of triglyceride metabolism in rodents but not in non-human primates, Cell Metabol. 27 (2018) 1236–1248, e6.
[35] T. Heinemeyer, E. Wingender, I. Reuter, H. Hermjakob, A.E. Kel, O.V. Kel, E. V. Ignatieva, E.A. Ananko, O.A. Podkolodnaya, F.A. Kolpakov, N.L. Podkolodny, N. A. Kolchanov, Databases on transcriptional regulation: TRANSFAC, TRRD and COMPEL, Nucleic Acids Res. 26 (1998) 362–367.
[36] M. Bléher, B. Meshko, I. Cacciapuoti, R. Gergondey, Y. Kovacs, D. Duprez, A. L'Honoré, E. Havis, Egr1 loss-of-function promotes beige adipocyte differentiation and activation specifically in inguinal subcutaneous white adipose tissue, Sci. Rep. 10 (2020) 15842.
[37] J. Han, E. Li, L. Chen, Y. Zhang, F. Wei, J. Liu, H. Deng, Y. Wang, The CREB coactivator CRTC2 controls hepatic lipid metabolism by regulating SREBP1, Nature 524 (2015) 243–246.
[38] M. Hatori, C. Vollmers, A. Zarrinpar, L. DiTacchio, E.A. Bushong, S. Gill, M. Leblanc, A. Chaix, M. Joens, J.A. Fitzpatrick, M.H. Ellisman, S. Panda, Time-restricted feeding without reducing caloric intake prevents metabolic diseases in mice fed a high-fat diet, Cell Metabol. 15 (2012) 848–860.
[39] M. Ruebel, K. Shankar, D. Gaddy, F. Lindsey, T. Badger, A. Andres, Maternal obesity is associated with ovarian inflammation and upregulation of early growth response factor 1, Am. J. Physiol. Endocrinol. Metab. 311 (2016) E269–E277.
[40] K.R. Chava, M. Karpurapu, D. Wang, M. Bhanoori, V. Kundumani-Sridharan, Q. Zhang, T. Ichiki, W.C. Glasgow, G.N. Rao, CREB-mediated IL-6 expression is required for 15(S)-hydroxyeicosatetraenoic acid-induced vascular smooth muscle cell migration, Arterioscler. Thromb. Vasc. Biol. 29 (2009) 809–815.
[41] T. Zarubin, J. Han, Activation and signaling of the p38 MAP kinase pathway, Cell Res. 15 (2005) 11–18.
[42] A. Cuenda, J. Rouse, Y.N. Doza, R. Meier, P. Cohen, T.F. Gallagher, P.R. Young, J. C. Lee, SB 203580 is a specific inhibitor of a MAP kinase homologue which is stimulated by cellular stresses and interleukin-1, FEBS Lett. 364 (1995) 229–233.
[43] V. Kundumani-Sridharan, J. Niu, D. Wang, D. Van Quyen, Q. Zhang, N.K. Singh, J. Subramani, S. Karri, G.N. Rao, 15(S)-hydroxyeicosatetraenoic acid-induced angiogenesis requires Src-mediated Egr-1-dependent rapid induction of FGF-2 expression, Blood 115 (2010) 2105–2116.
[44] E. Daveri, E. Cremonini, A. Mastaloudis, S.N. Hester, S.M. Wood, A.L. Waterhouse, M. Anderson, C.G. Fraga, P.I. Oteiza, Cyanidin and delphinidin modulate inflammation and altered redox signaling improving insulin resistance in high fat-fed mice, Redox Biol 18 (2018) 16–24.
[45] G. Vial, H. Dubouchaud, K. Couturier, C. Cottet-Rousselle, N. Taleux, A. Athias, A. Galinier, L. Casteilla, X.M. Leverve, Effects of a high-fat diet on energy metabolism and ROS production in rat liver, J. Hepatol. 54 (2011) 348–356.
[46] A.G. Barata, T.P. Dick, A role for peroxiredoxins in H_2O_2- and MEKK-dependent activation of the p38 signaling pathway, Redox Biol 28 (2020) 101340.
[47] R. Bretón-Romero, S. Lamas, Hydrogen peroxide signaling mediator in the activation of p38 MAPK in vascular endothelial cells, Methods Enzymol. 528 (2013) 49–59.
[48] W. Li, Z. Ma, J. Ma, X. Li, Q. Xu, W. Duan, X. Chen, Y. Lv, S. Zhou, E. Wu, Q. Ma, X. Huo, Hydrogen peroxide mediates hyperglycemia-induced invasive activity via ERK and p38 MAPK in human pancreatic cancer, Oncotarget 6 (2015) 31119–31133.
[49] B. Turner-Ivey, Y. Manevich, J. Schulte, E. Kistner-Griffin, A. Jezierska-Drutel, Y. Liu, C.A. Neumann, Role for Prdx1 as a specific sensor in redox-regulated senescence in breast cancer, Oncogene 32 (2013) 5302–5314.
[50] E.E. Kelley, N.K. Khoo, N.J. Hundley, U.Z. Malik, B.A. Freeman, M.M. Tarpey, Hydrogen peroxide is the major oxidant product of xanthine oxidase, Free Radic. Biol. Med. 48 (2010) 493–498.
[51] S. Guthikonda, C. Sinkey, T. Barenz, W.G. Haynes, Xanthine oxidase inhibition reverses endothelial dysfunction in heavy smokers, Circulation 107 (2003) 416–421.
[52] W. Dubiel, D. Dubiel, D.A. Wolf, M. Naumann, Cullin 3-based ubiquitin ligases as master regulators of mammalian cell differentiation, Trends Biochem. Sci. 43 (2018) 95–107.
[53] J. Heeren, L. Scheja, Metabolic-associated fatty liver disease and lipoprotein metabolism, Mol. Metab. 20 (2021) 101238.
[54] C.J. Packard, T. Demant, J.P. Stewart, D. Bedford, M.J. Caslake, G. Schwertfeger, A. Bedynek, J. Shepherd, D. Seidel, Apolipoprotein B metabolism and the distribution of VLDL and LDL subfractions, J. Lipid Res. 41 (2000) 305–318.
[55] R.H. Unger, Y.T. Zhou, Lipotoxicity of beta-cells in obesity and in other causes of fatty acid spillover, Diabetes 50 Suppl 1 (2001) S118–S121.
[56] R.M. Bell, R.A. Coleman, Enzymes of glycerolipid synthesis in eukaryotes, Annu. Rev. Biochem. 49 (1980) 459–487.
[57] S. Cases, S.J. Smith, Y.W. Zheng, H.M. Myers, S.R. Lear, E. Sande, S. Novak, C. Collins, C.B. Welch, A.J. Lusis, S.K. Erickson, R.V. Farese Jr., Identification of a gene encoding an acyl CoA:diacylglycerol acyltransferase, a key enzyme in triacylglycerol synthesis, Proc. Natl. Acad. Sci. U.S.A. 95 (1998) 13018–13023.
[58] S.J. Smith, S. Cases, D.R. Jensen, H.C. Chen, E. Sande, B. Tow, D.A. Sanan, J. Raber, R.H. Eckel, R.V. Farese Jr., Obesity resistance and multiple mechanisms of triglyceride synthesis in mice lacking Dgat, Nat. Genet. 25 (2000) 87–90.
[59] S. Cases, S.J. Stone, P. Zhou, E. Yen, B. Tow, K.D. Lardizabal, T. Voelker, R. V. Farese Jr., Cloning of DGAT2, a second mammalian diacylglycerol acyltransferase, and related family members, J. Biol. Chem. 276 (2001) 38870–38876.
[60] P. Oelkers, A. Behari, D. Cromley, J.T. Billheimer, S.L. Sturley, Characterization of two human genes encoding acyl coenzyme A:cholesterol acyltransferase-related enzymes, J. Biol. Chem. 273 (1998) 26765–26771.
[61] H.C. Chen, S.J. Smith, Z. Ladha, D.R. Jensen, L.D. Ferreira, L.K. Pulawa, J. G. McGuire, R.E. Pitas, R.H. Eckel, R.V. Farese Jr., Increased insulin and leptin sensitivity in mice lacking acyl CoA:diacylglycerol acyltransferase 1, J. Clin. Invest. 109 (2002) 1049–1055.
[62] S.J. Stone, H.M. Myers, S.M. Watkins, B.E. Brown, K.R. Feingold, P.M. Elias, R. V. Farese Jr., Lipopenia and skin barrier abnormalities in DGAT2-deficient mice, J. Biol. Chem. 279 (2004) 11767–11776.
[63] R. Chattopadhyay, A.M. Mani, N.K. Singh, G.N. Rao, Resolvin D1 blocks H_2O_2-mediated inhibitory crosstalk between SHP2 and PP2A and suppresses endothelial-monocyte interactions, Free Radic. Biol. Med. 117 (2018) 119–131.
[64] P. Pichavaram, A.M. Mani, N.K. Singh, G.N. Rao, Cholesterol crystals promote endothelial cell and monocyte interactions via H2O2-mediated PP2A inhibition, NFκB activation and ICAM1 and VCAM1 expression, Redox Biol 24 (2019) 101180.
[65] T. Ichiki, T. Tokunou, K. Fukuyama, N. Iino, S. Masuda, A. Takeshita, Cyclic AMP response element-binding protein mediates reactive oxygen species-induced c-fos expression, Hypertension 42 (2003) 177–183.
[66] J.C. Juarez, M. Manuia, M.E. Burnett, O. Betancourt, B. Boivin, D.E. Shaw, N. K. Tonks, A.P. Mazar, F. Doñate, Superoxide dismutase 1 (SOD1) is essential for H2O2-mediated oxidation and inactivation of phosphatases in growth factor signaling, Proc. Natl. Acad. Sci. U.S.A. 105 (2008) 7147–7152.
[67] H.C. Patterson, C. Gerbeth, P. Thiru, N.F. Vögtle, M. Knoll, A. Shahsafaei, K. E. Samocha, C.X. Huang, M.M. Harden, R. Song, C. Chen, J. Kao, J. Shi, W. Salmon, Y.D. Shaul, M.P. Stokes, J.C. Silva, G.W. Bell, D.G. MacArthur, J. Ruland, C. Meisinger, H.F. Lodish, A respiratory chain controlled signal transduction cascade in the mitochondrial intermembrane space mediates hydrogen peroxide signaling, Proc. Natl. Acad. Sci. U.S.A. 112 (2015) E5679–E5688.
[68] P. Richette, C. Poitou, P. Manivet, J. Denis, J.L. Bouillot, K. Clément, J.M. Oppert, T. Bardin, Weight loss, xanthine oxidase, and serum urate levels: a prospective longitudinal study of obese patients, Arthritis Care Res. 68 (2016) 1036–1042.
[69] H.K. Tam, A.S. Kelly, C.K. Fox, B.M. Nathan, L.A. Johnson, Weight loss mediated reduction in xanthine oxidase activity and uric acid clearance in adolescents with severe obesity, Child. Obes. 12 (2016) 286–291.
[70] D.B. Harmon, W.K. Mandler, I.J. Sipula, N. Dedousis, S.E. Lewis, J.T. Eckels, J. Du, Y. Wang, B.R. Huckestein, P.J. Pagano, E. Cifuentes-Pagano, G.E. Homanics, T. J. Van't Erve, M. Stefanovic-Racic, M.J. Jurczak, R.M. O'Doherty, E.E. Kelley, Hepatocyte-specific ablation or whole-body inhibition of xanthine oxidoreductase in mice corrects obesity-induced systemic hyperuricemia without improving metabolic abnormalities, Diabetes 68 (2019) 1221–1229.
[71] T. Nishikawa, N. Nagata, T. Shimakami, T. Shirakura, C. Matsui, Y. Ni, F. Zhuge, L. Xu, G. Chen, M. Nagashimada, T. Yamashita, Y. Sakai, T. Yamashita, E. Mizukoshi, M. Honda, S. Kaneko, T. Ota, Xanthine oxidase inhibition attenuates insulin resistance and diet-induced steatohepatitis in mice, Sci. Rep. 10 (2020) 815.
[72] J.D. Horton, J.L. Goldstein, M.S. Brown, SREBPs: activators of the complete program of cholesterol and fatty acid synthesis in the liver, J. Clin. Invest. 109 (2002) 1125–1131.
[73] F.W. Sanders, J.L. Griffin, De novo lipogenesis in the liver in health and disease: more than just a shunting yard for glucose, Biol. Rev. Camb. Phil. Soc. 91 (2016) 452–468.
[74] M. Yang, M. Zhang, Q. Liu, T. Xu, T. Huang, D. Yao, C.W. Wong, J. Liu, M. Guan, 18β-Glycyrrhetinic acid acts through hepatocyte nuclear factor 4 alpha to modulate lipid and carbohydrate metabolism, Pharmacol. Res. 157 (2020) 104840.
[75] K. Fujita, Y. Nozaki, K. Wada, M. Yoneda, Y. Fujimoto, M. Fujitake, H. Endo, H. Takahashi, M. Inamori, N. Kobayashi, H. Kirikoshi, K. Kubota, S. Saito, A. Nakajima, Dysfunctional very-low-density lipoprotein synthesis and release is a key factor in nonalcoholic steatohepatitis pathogenesis, Hepatology 50 (2009) 772–780.
[76] Y.J. Choi, H.S. Shin, H.S. Choi, J.W. Park, I. Jo, E.S. Oh, K.Y. Lee, B.H. Lee, R. J. Johnson, D.H. Kang, Uric acid induces fat accumulation via generation of endoplasmic reticulum stress and SREBP-1c activation in hepatocytes, Lab. Invest. 94 (2014) 1114–1125.
[77] M.A. Lanaspa, L.G. Sanchez-Lozada, Y.J. Choi, C. Cicerchi, M. Kanbay, C.A. Roncal-Jimenez, T. Ishimoto, N. Li, G. Marek, M. Duranay, G. Schreiner, B. Rodriguez-Iturbe, T. Nakagawa, D.H. Kang, Y.Y. Sautin, R.J. Johnson, Uric acid induces hepatic steatosis by generation of mitochondrial oxidative stress: potential role in fructose-dependent and -independent fatty liver, J. Biol. Chem. 287 (2012) 40732–40744.
[78] M. Su, L. Sun, W. Li, H. Liu, Y. Liu, Y. Wei, Y. Yuan, L. Zheng, S. Yin, C. Dai, C. Zhao, Z. Pan, Y. Li, Metformin alleviates hyperuricaemia-induced serum FFA elevation and insulin resistance by inhibiting adipocyte hypertrophy and reversing suppressed white adipose tissue beiging, Clin. Sci. (Lond). 134 (2020) 1537–1553.
[79] A.M. Giudetti, F. Damiano, G.V. Gnoni, L. Siculella, Low level of hydrogen peroxide induces lipid synthesis in BRL-3A cells through a CAP-independent SREBP-1a activation, Int. J. Biochem. Cell Biol. 45 (2013) 1419–1426.
[80] M. Sekiya, A. Hiraishi, M. Touyama, K. Sakamoto, Oxidative stress induced lipid accumulation via SREBP1c activation in HepG2 cells, Biochem. Biophys. Res. Commun. 375 (2008) 602–607.

[81] J.N. Livingston, P.A. Gurny, D.H. Lockwood, Insulin-like effects of polyamines in fat cells. Mediation by H_2O_2 formation, J. Biol. Chem. 252 (1977) 560–562.
[82] J.C. Lawrence Jr., J. Larner, Activation of glycogen synthase in rat adipocytes by insulin and glucose involves increased glucose transport and phosphorylation, J. Biol. Chem. 253 (1978) 2104–2113.
[83] S.D. Parlee, S.I. Lentz, H. Mori, O.A. MacDougald, Quantifying size and number of adipocytes in adipose tissue, Methods Enzymol. 537 (2014) 93–122.
[84] L. McAllan, K.R. Maynard, A.S. Kardian, A.S. Stayton, S.L. Fox, E.J. Stephenson, C. E. Kinney, N.K. Alshibli, C.K. Gomes, J.F. Pierre, M.A. Puchowicz, D. Bridges, K. Martinowich, J.C. Han, Disruption of brain-derived neurotrophic factor production from individual promoters generates distinct body composition phenotypes in mice, Am. J. Physiol. Endocrinol. Metab. 315 (2018) E1168–E1184.
[85] I.R. Bederman, S. Foy, V. Chandramouli, J.C. Alexander, S.F. Previs, Triglyceride synthesis in epididymal adipose tissue: contribution of glucose and non-glucose carbon sources, J. Biol. Chem. 284 (2009) 6101–6108.
[86] D.Z. Brunengraber, B.J. McCabe, T. Kasumov, J.C. Alexander, V. Chandramouli, S. F. Previs, Influence of diet on the modeling of adipose tissue triglycerides during growth, Am. J. Physiol. Endocrinol. Metab. 285 (2003) E917–E925.
[87] S.Y. Cheranov, M. Karpurapu, D. Wang, B. Zhang, R.C. Venema, G.N. Rao, An essential role for SRC-activated STAT-3 in 14,15-EET-induced VEGF expression and angiogenesis, Blood 111 (2008) 5581–5591.
[88] N.K. Singh, S. Kotla, R. Kumar, G.N. Rao, Cyclic AMP response element binding protein mediates pathological retinal neovascularization via modulating DLL4-NOTCH1 signaling, EBioMedicine 2 (2015) 1767–1784.
[89] K.L. Berkner, Development of adenovirus vectors for the expression of heterologous genes, Biotechniques 6 (1988) 616–629.
[90] S. Govatati, P. Pichavaram, J. Janjanam, B. Zhang, N.K. Singh, A.M. Mani, J. G. Traylor Jr., A.W. Orr, G.N. Rao, NFATc1-E2F1-LMCD1-Mediated IL-33 expression by thrombin is required for injury-induced neointima formation, Arterioscler. Thromb. Vasc. Biol. 39 (2019) 1212–1226.